Symmetry breaking of azimuthal thermo-acoustic modes in annular cavities: a theoretical study

M Bauerheim, P Salas, Franck Nicoud, Thierry Poinsot

Symmetry breaking of azimuthal thermo-acoustic modes in annular cavities: a theoretical study

M. Bauerheim[1]†, P. Salas[2], F. Nicoud[3] and T. Poinsot[4]

[1]CERFACS, CFD team, 42 Av Coriolis, 31057 Toulouse, France

[2]INRIA Bordeaux - Sud Ouest, HiePACS Project, joint INRIA-CERFACS lab. on High Performance Computing

[3]Université Montpellier 2. I3M UMR CNRS 5149

[4]IMF Toulouse, INP de Toulouse and CNRS, 31400 Toulouse , France

(Received ?; revised ?; accepted ?. - To be entered by editorial office)

A large range of physical problems containing rotating symmetry exhibit azimuthal waves, from electromagnetic waves in nano photonics crystal to seismic waves in giant stars. When this symmetry is broken, clockwise and counter-clockwise waves are split into two distinct modes which can become unstable. This paper focuses on a theoretical study of symmetry breaking in annular cavities containing N flames prone to azimuthal thermo-acoustic instabilities. A general dispersion relation for not perfectly axisymmetric cavities is obtained and analytically solved when coupling factors are small. It provides an explicit expression of the frequencies and growth rates of all azimuthal modes of the configuration. This analytical study unveils two parameters affecting the stability of the mode: (1) a coupling strength corresponding to a mean flame effect and (2) a splitting strength due to the symmetry breaking when flames are different. This theory has been validated using a 3D Helmholtz solver and a good agreement is found. When only two types of flames are introduced in the annular cavity, the splitting strength is found to depend independently on two parameters: the difference between the two burner types and the pattern used to distribute the flames along the azimuthal direction. To first-order, this theory suggests that the most stable configuration is obtained for perfectly axisymmetric configuration. Therefore, breaking symmetry by mixing different flames cannot improve the stability of the annular combustor independently of the flame distribution pattern.

Key words: azimuthal modes ; analytical ; combustion instabilities ; symmetry ; control

† Email address for correspondence: bauerheim@cerfacs.fr

Nomenclature

α_i Normalized abscissa of the i^{th} flame
ϵ Wavenumber perturbation
$\gamma(\pm 2p)$ $\pm 2p^{th}$ Fourier coefficient of the FTF distribution
Γ_i Coupling parameter of the i^{th} burner
λ Acoustic wavelength
$\mathcal{K}$ Reduced splitting strength
$\mathcal{S}_0$ Splitting strength
ω Angular frequency
ρ^0 Mean density of the hot gas
ρ_u^0 Mean density of the cold gas
Σ_0 Coupling strength
τ_i FTF time-delay of the i^{th} burner
θ Azimuthal angle in the annular cavity
c^0 Mean sound speed in the hot gas
c_u^0 Mean sound speed in the cold gas
f complex frequency
$k = \omega/c^0$ Wavenumber
L_c and R_c Half perimeter and radius of the annular chamber
L_i Length of the i^{th} burner
N Number of burners
n_i FTF amplitude of the i^{th} burner
p Azimuthal mode order
p_i' Pressure fluctuations in the annular cavity
$p_{b,i}'$ Pressure fluctuations in the i^{th} burner
$q^{\pm} = p' \pm \rho^0 c^0 u'$ Acoustic propagating waves
R_i Propagation matrix of the i^{th} annular sector
S_c Cross section of the annular chamber
S_i Section of the i^{th} burner
T_i Interaction matrix
u_i' Azimuthal velocity fluctuations in the annular cavity
$w_{b,i}'$ Axial velocity fluctuations in the i^{th} burner
z Axial coordinate in the burners
Z_i Upstream impedance of the i^{th} burner
Z_{tr} Translated or equivalent impedance of the burner and flame
ANR Annular Network Reduction
ATACAMAC Analytical Tool to Analyze and Control Azimuthal Mode in Annular Combustor
FTF Flame Transfer Function

1. Introduction

A wide range of physical problems, from nano photonics crystal (Borisnika 2006) and molecules (Creighton 1982) to giant stars (Lavely 1983), take place in torus or disks: they contain rotating symmetries and can therefore exhibit azimuthal/transverse oscillations such as electromagnetic waves (Pang *et al.* 2007), acoustic waves (Krebs *et al.* 2002; Noiray *et al.* 2011; Parmentier *et al.* 2012; Bauerheim *et al.* 2014*b*), surface waves (Feng & Sethna 1989; Simonelli & Gollub 1989), magneto static spin-waves† (Hoffmann *et al.*

† Spin waves are propagating disturbances in the ordering of magnetic materials.

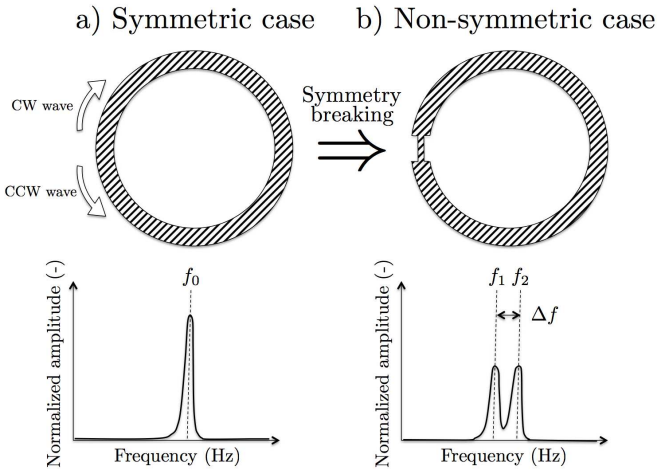

FIGURE 1. a) Sketch of a configuration with rotating symmetries (top) and its associated spectrum (bottom). Two waves (clockwise (CW) and counter-clockwise (CCW)) can exist and have the same frequency f_0: the mode is "degenerate". When the rotating symmetry is broken (b), the degenerate mode at f_0 is split into two distinct waves with different yet close frequencies f_1 and f_2 (bottom).

2007; Guslienko *et al.* 2008; Barman *et al.* 2010; Kammerer *et al.* 2011) or solid vibrations (Creighton 1982; Perrin & Charnley 1973; Lin & Parker 2000*a*,*b*; Kumar & Krousgrill 2012). When the rotating symmetry is perfect, these modes occur in doubly-degenerate pairs with two independent oscillations (a clockwise and a counter-clockwise waves) at the same frequency (a, in figure 1, left). However, when systems with rotational symmetry are modified either in their geometry or by spatially varying their properties or their boundary conditions, degenerate pairs can split into two distinct modes with different yet close frequencies (b, in figure 1, right). In some applications, the splitting frequency Δf can be fairly large and therefore cannot be ignored (e.g. $\Delta f = 0.25\ GHz$ for spin-wave modes in small ferromagnetic elements (Hoffmann *et al.* 2007)).

In many applications, this splitting can lead to catastrophic effects, requiring studies to understand their underlying nature and methods to suppress them. For instance, photonics crystal (i.e. devices where several electromagnetically micro cavities are coupled with a specific pattern to form "photon molecules") with high quality-factor are essential for the development of the next generation of optoelectronic components but undesired symmetry breaking and associated non-degenerate modes reduce their overall performances. To tackle this problem, Borisnika (2006) proposed arrangement patterns with enhanced symmetry characteristics which reduce effects of non-degenerate modes and improve the quality factors of the devices.

In applications based on magnetic disks which exhibit spin-waves (Hoffmann *et al.* 2007; Guslienko *et al.* 2008; Barman *et al.* 2010; Kammerer *et al.* 2011), theoretical models show that the splitting is a consequence of the interaction of the azimuthal mode with the vortex core gyrotropic motion. Both simulations and experiments have confirmed that removing the vortex core from the disk suppresses mode splitting (Hoffmann *et al.* 2007). This suggests that theory, simulations or experiments can unveil the splitting origins and offer methods to suppress them.

In configurations where symmetry breaking is well described theoretically (Mazzei *et al.* 2007), scientists can willingly perform symmetry breaking to analyze the phenomenon

responsible for this splitting. For example, in ultra-high quality factor whispering gallery mode resonators (WGMs), a small imperfection (similar to the case b in figure 1) or a deposited particle can scatter light from one of the two cavity modes (counter-clockwise for instance) into free space as well as in the opposite direction (i.e. clockwise). Scientists can then exploit this splitting to accurately determine particle sizes (Mazzei *et al.* 2007; Kippenberg 2010). A similar methodology is used in helioseismology (Lavely 1983; Kosovichev 1999; Tripathy *et al.* 2000) where the internal solar structure and dynamics can be inferred from observed frequencies which can be split either by rotation, asphericity or the magnetic field of the star.

In the particular field of fluid mechanics, symmetry breaking phenomena are less studied due to complex geometries, high non-linear levels and complex physics. In simple configurations (square and quasi-square channels), such a splitting effect has been studied for surface waves (Feng & Sethna 1989; Simonelli & Gollub 1989). Results show that the symmetry of the configuration has dramatic effects on the dynamics. The degenerate case yields no time-dependent patterns. However, setups where the two components are separated in frequency, even by a small amount (about 1%), can lead to chaotic states (Simonelli & Gollub 1989). Similarly Davey et al. (Davey & Salwen 1994) investigate the linear stability of the first circumferential mode in both a circular and an elliptic pipe. They show analytically that the circular problem has a double degenerate eigenvalue f_0 while the ellipticity of the latter configuration splits the doublets into two distinct eigenvalues $f_0 \pm \Delta f/2$. The imaginary part of the splitting frequency Δf is non-zero and thus the ellipticity of the cross-sectional area always makes the flow less stable. This splitting mechanism induced by the symmetry reduction (from the axisymmetry group S^1 of the circular problem to the mirror symmetry group Z_2 associated to the elliptic cross-section) is briefly discussed in its fundamental mathematical aspects in (Guckenheimer & Mahalov 1992) and applied to the instability of a vortex filament in a non-circular cylinder. Such a symmetry reduction also plays a crucial role on the oscillations of droplets due to a-sphericity (Cummings & Blackburn 1991) and/or Coriolis forces if the droplet is rotating (Busse 1984).

Recently, symmetry breaking has been also investigated in complex annular gas turbines (figure 2) (Noiray *et al.* 2011; Parmentier *et al.* 2012) which exhibit azimuthal acoustic waves produced by thermo-acoustic instabilities (O'Connor & Lieuwen 2014 - under review). Such combustion instabilities remain a severe problem in the development of modern gas turbines. Lean premixed combustors, designed to reduce significantly nitric oxides emissions are especially prone to these oscillations which can lead to vibrations and structural damage (Lieuwen & Yang 2005; Schuermans *et al.* 2003; Krebs *et al.* 2002). These unsteady phenomena come from the interaction between acoustics and heat release fluctuations which act as a volume acoustic source (Strahle 1972). In annular combustion chambers (figure 2), these instabilities often take the form of azimuthal modes (Schuermans *et al.* 2003; Krebs *et al.* 2002; Parmentier *et al.* 2012; Bauerheim *et al.* 2014*b*; Worth & Dawson 2013*a*,*b*).

In real engines, usually, identical burners are distributed regularly along the azimuthal direction (figure 2). Therefore, perfectly axisymmetric configurations have been intensively investigated using theoretical (Parmentier *et al.* 2012; Bauerheim *et al.* 2014*b*; Stow & Dowling 2001; Pankiewitz & Sattelmayer 2003; Stow & Dowling 2003), acoustic and LES tools (Evesque & Polifke 2002; Kopitz *et al.* 2005; Staffelbach *et al.* 2009; Wolf *et al.* 2012) and more rarely experiments (Krebs *et al.* 2002; Worth & Dawson 2013*b*,*a*; Bourgouin *et al.* 2013). Annular chambers exhibit specific azimuthal modes which can be standing or spinning in the azimuthal direction (Evesque *et al.* 2003; Sensiau *et al.* 2009). Azimuthal modes are often "degenerate": two modes are found at the same frequency

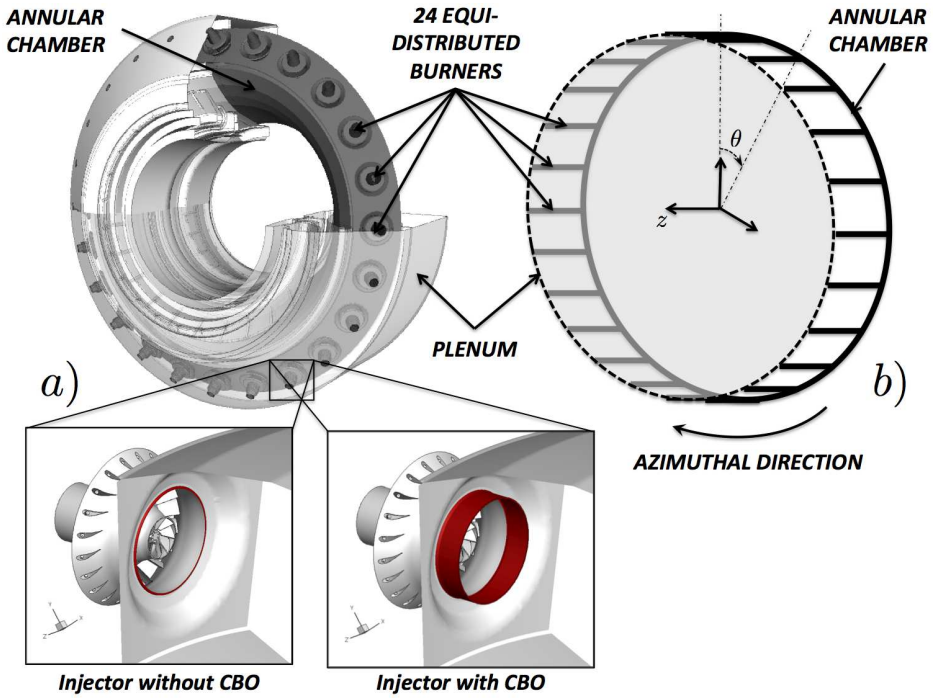

FIGURE 2. a) A typical 3D configuration of an industrial annular combustion chamber equipped with $N = 24$ burners with or without CBO and b) Network model of the annular chamber (———) with $N = 24$ burners. The annular plenum (- - -) is removed for the sake of simplicity.

(two counter-rotating spinning modes for example). These two modes can combine and switch, leading to combustors which exhibit standing, spinning or mixed modes for various times, changing from one mode to another one at random instants. The simultaneous existence of these modes was observed numerically (Wolf *et al.* 2012) and experimentally in laboratory setups (Worth & Dawson 2013*b*; Bourgouin *et al.* 2013) and even in real gas turbines (Krebs *et al.* 2002). Mode switching has been postulated to be due to random turbulent fluctuations (Noiray & Schuermans 2013). Azimuthal modes are not necessarily degenerate leading to a more complicated situation where the configuration is strongly affected by symmetry modifications as shown by studies of sound produced by bells (Perrin & Charnley 1973) where non-degenerate but very close azimuthal modes (also called "non-degenerate singlets") lead to "warble", an undesired modulation due to the coupling of two modes with different but very close frequencies.

The effect of asymmetry on the eigenfrequencies and nature of azimuthal modes in annular chambers is still an open question. Earlier work of Oefelein & Yang (1993) focused on symmetry breaking using baffles to prevent combustion instabilities in the F-1 rocket engines. They suggested that asymmetry can be introduced to control unstable modes using passive techniques. Stow & Dowling (2003) applied azimuthal variations using Helmholtz resonators on an annular academical test bench. Similarly, Berenbrink & Hoffmann (2001) and Krueger *et al.* (2000) (reviewed by Culick & Kuentzmann (2006)) broke the symmetry of an annular engine by using CBOs (Cylindrical Burner Outlet, figure 2-a, bottom) to modify the time-delay τ_i of some of the 24 flames and control instabilities in a $N = 24$ burners industrial combustor. They varied the number of CBOs installed among the 24 burners showing that adding CBOs improved stability. However, it was not clear if the stabilization was due to the CBO devices rather than, as argued by the authors, to

symmetry breaking in this particular case. Lately, Moeck *et al.* (2010) and Gelbert *et al.* (2012) carried out an annular Rijke experiment with heating grids acting like flames. They introduced circumferential variations through asymmetric power distributions of the grids to modify the azimuthal modes behavior and noticed that the staging pattern can split degenerate azimuthal modes (doublets) into non-degenerate pairs (singlets) as suggested in (Perrin & Charnley 1973) for bells if the system's symmetry is changed. **Recently, experimental (Worth & Dawson 2013*b*,*a*) and theoretical (Bauerheim *et al.* 2014*a*) studies have shown that the azimuthal flow itself can break the rotating symmetry. This flow gyration can be generated by the compressor or diffuser outlet, by the swirlers or even by effusive plates in modern gas turbines. Worth & Dawson (2013*a*,*b*) have shown that changing the rotating direction of some swirlers can modify the stability and the structure of the observed acoustic mode. This mean flow effect has been analytically unveiled by Bauerheim *et al.* (2014*a*) demonstrating that the mean azimuthal Mach number is one parameter controlling the symmetry breaking affecting both the stability and the mode nature.**

A few theories consider the effect of asymmetry on the existence and nature of azimuthal modes (standing, spinning or mixed). Schuermans *et al.* (2006) suggest that standing modes are observed for low amplitudes but that, at higher amplitudes, one of the two rotating modes eventually dominates. However, Sensiau *et al.* (2009) have shown that even in the linear regime, any change in symmetry can lead to the appearance of one rotating mode dominating the other one: when the symmetry of the configuration is broken, the standing azimuthal mode is changed into two counter-rotating azimuthal modes with different growth rates so that one of them eventually dominates the other. Noiray *et al.* (2011) have proved that the $2p^{th}$ Fourier coefficient of the heat release, temperature or even acoustic losses azimuthal distribution (where p is the order of the azimuthal mode considered) strongly impacts the frequency as well as the mode nature on an annular rig. Dawson et al. (Worth & Dawson 2013*b*,*a*) have also shown that the modes nature can result from the interaction with the mean flow by breaking symmetry thanks to clockwise/anti-clockwise swirlers: they observed a strong correlation between the bulk swirl direction and the direction of spin.

Noiray *et al.* (2011) used an analytical formulation to study the effect of asymmetry on a annular rig with a circumferential distribution of heat release, temperature and acoustic losses. However for the sake of simplicity, this annular rig was simplified and contained no burner at all: no study was conducted on annular chambers connected to burners, a configuration which is more realistic of real gas turbines but more difficult to formulate analytically.

The present paper describes an analytical approach to investigate the effects of symmetry breaking on azimuthal modes in an annular chamber fed by N identical or non-identical burners. This configuration called BC (Burner+Chamber, figure 3) allows the investigation of asymmetry's effect on eigenfrequencies and nature of circumferential modes. The model is based on a network description (figure 2) of the combustion chamber where only plane acoustic waves travel and interact with flames (Parmentier *et al.* 2012). It allows to take into account the effects of burners and of complex flame models while providing a solution which remains almost fully analytical. This analytical formulation reveals which parameters control the growth and the nature of the modes, something which would be impossible with a numerical approach.

This paper is organized as follows: Section 2 briefly describes the principle of the acoustic network model called ATACAMAC ("Analytical Tool to Analyze and Control Azimuthal Modes in Annular Combustors") and how an analytical dispersion relation

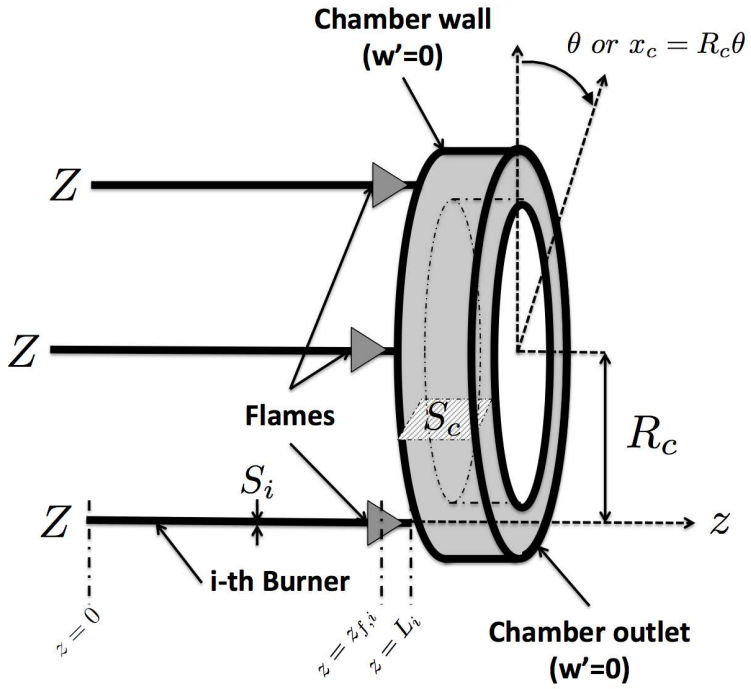

FIGURE 3. BC configuration to study unstable modes in annular chambers

can be obtained in such a configuration (Parmentier *et al.* 2012). In Section 3, analytical calculations of eigenfrequencies are presented for both an "unperturbed" case (an annular cavity without flames) and for a general non-symmetric BC configuration (figure 3). Section 4 describes the test cases as well as the 3D Helmholtz solver used to validate the ATACAMAC results. Two application cases are presented : an academic chamber with $N = 3$ burners and a real configuration with $N = 24$ burners (figure 2). In Section 5, ATACAMAC is applied to a BC configuration with $N = 3$ identical burners (Section 5.1) and then $N = 3$ different burners (Section 5.2), highlighting the effect of circumferential patterns on eigenfrequencies and modes nature. ATACAMAC results are systematically compared to those provided by a 3D acoustic code solving the complete acoustic equations in three dimensions in the low Mach number case (Nicoud *et al.* 2007; Silva *et al.* 2013; Selle *et al.* 2006; Sensiau *et al.* 2009). Finally, Section 6 presents the effects of asymmetry on instabilities in a $N = 24$ burners configuration typical of real engines. Results are compared to observations made in real gas turbine engines (Berenbrink & Hoffmann 2001; Krueger *et al.* 2000).

2. A network model for a BC (Burner+Chamber) non-symmetric configuration

2.1. *Model description*

This study focuses on a BC (Burners+Chamber) configuration where an annular chamber is fed by N burners (figure 3). An impedance Z is imposed at the upstream end of each burner. Mean density and sound speed are noted ρ^0 and c^0 in the annular chamber and ρ_u^0 and c_u^0 for the unburnt mixture in the N burners. The perimeter and the **cross sectional area (perpendicular to the azimuthal direction)** of the annular chamber

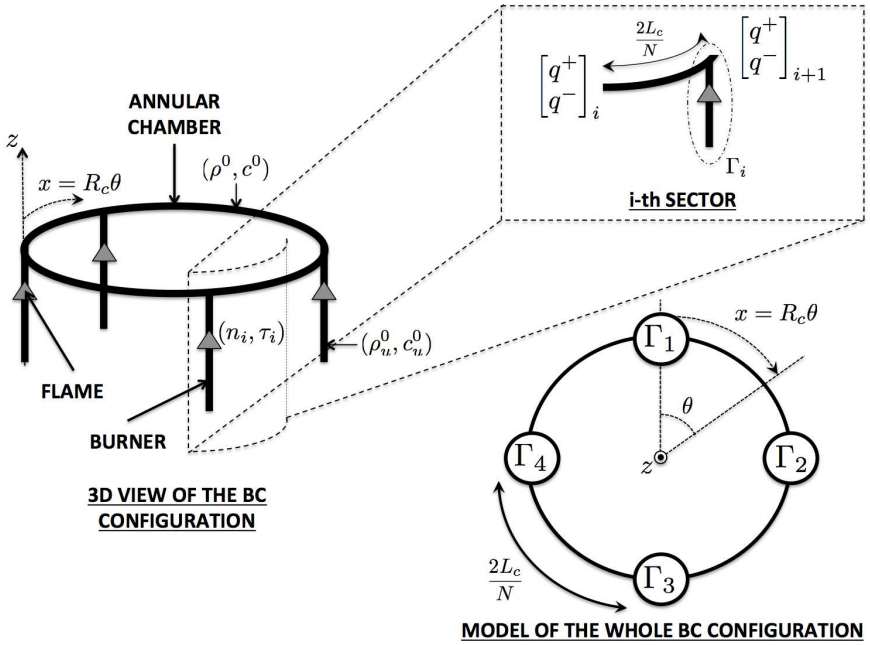

FIGURE 4. 3D view of a BC configuration with $N = 4$ burners (left), zoom on the i^{th} sector (top right) and model of the whole BC configuration (bottom right) where Γ_i represents the burner/chamber interaction (Parmentier *et al.* 2012)

are noted $2L_c = 2\pi R_c$ and S_c respectively. The length and section of the i^{th} burner are L_i and S_i. The position along the annular cavity is given by the angle θ defining an abscissa $x_c = R_c\theta$. The location of the flames is similar in all burners and is given by the normalized abscissa $\alpha = z_{f,i}/L_i$ (figure 3).

This model corresponds to situations where pressure fluctuations in the combustion chamber depend on the angle θ (or the azimuthal position x) but not on the axial direction z in the chamber (they depend on the coordinate z only in the burners). This case can be observed in combustors terminated by choked nozzles which acoustically behave almost like a rigid wall (i.e. $u' = 0$ under the low upstream Mach number assumption (Marble & Candel 1977)). Since the chamber inlet is also close to a velocity node, modes which have no variation along z can develop in the chamber, as shown by recent LES in real engines (Wolf *et al.* 2009).

The model provides the analytical expression of eigenfrequencies for a general asymmetric case for any mode order p and any number of burners N as well as general rules on stability for annular combustors. Results on structure and nature of azimuthal modes (spinning, standing or mixed) will be derived using this analytical study to show how asymmetry can promote specific modes and control instabilities (Worth & Dawson 2013*b*,*a*; Moeck *et al.* 2010; Gelbert *et al.* 2012; Noiray *et al.* 2011).

2.2. *Annular Network Reduction (ANR)*

Network models which account for one annular cavity connected to N burners usually require a large number of unknown variables (acoustic pressure and velocity in each network tube) and a large matrix describing the system (typically a $2N$-by-$2N$ matrix). To reduce the size of the system (i.e. a matrix of size 2-by-2, independent of the number N of burners), the ANR (Annular Network Reduction) methodology proposed in (Bauer-

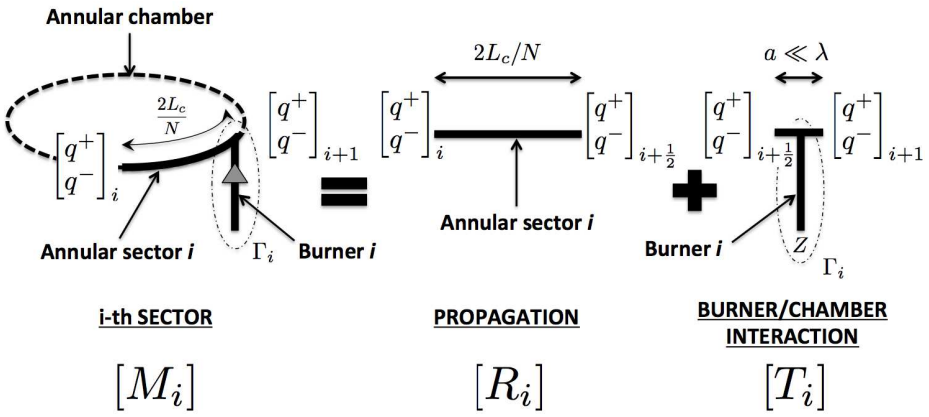

FIGURE 5. ANR methodology: each sector is decomposed into a free propagation of azimuthal waves (characteristic length $2L_c/N$) and a compact burner/chamber interaction (characteristic length $a \ll \lambda$) modeled by the coupling parameter Γ_i

heim *et al.* 2014*b*) is applied: the full annular combustor is split into N sectors which differ only via the burner/chamber junction (figures 4 and 5). Between each sector, the propagation of azimuthal waves (along θ or x) can be modeled by a transfer matrix R_i as proposed by Parmentier *et al.* (2012) (figure 5, propagation):

$$\begin{bmatrix} q^+ \\ q^- \end{bmatrix}_{i+\frac{1}{2}} = \begin{bmatrix} R_i \end{bmatrix} \begin{bmatrix} q^+ \\ q^- \end{bmatrix}_i \text{ where } \begin{bmatrix} R_i \end{bmatrix} = \begin{bmatrix} W & 0 \\ 0 & \frac{1}{W} \end{bmatrix} \tag{2.1}$$

where $q^{\pm} = p' \pm \rho^0 c^0 u'$, $W = e^{2jkL_c/N}$ and the wavenumber $k = \omega/c^0$.

The area where the i^{th} burner is connected to the annular chamber (`---` in figure 4, top right) was investigated by O'Connor et al. (O'Connor & T.Lieuwen 2012; J.O'Connor & T.Lieuwen 2012*b*,*a*) and can be assumed to be compact: $a \ll \lambda$**, where** $a = 2\sqrt{S_i/\pi}$ **is the burner diameter and** $\lambda = 2L_c/p$ **is the acoustic wavelength leading to the compactness criterion** $p \ll L_c\sqrt{\pi/S_c} \simeq 116$**.** As shown in figure 6, using the equations of acoustic propagation in the cold ($0 < z < \alpha L_i$) and hot ($\alpha L_i < z < L_i$) parts of the burner as well as the jump conditions through the i^{th} flame ($z = \alpha L_i$), the effect of the whole i^{th} burner on the annular chamber can be obtained by a translated impedance from $z = 0$ (impedance Z) to the burner/chamber junction at $z = L_i$ (impedance $Z_{tr} = \frac{p'_{b,i}(z=L_i)}{\rho^0 c^0 w'_{b,i}(z=L_i)}$) (Bauerheim *et al.* 2014*b*; Blimbaum *et al.* 2012):

$$Z_{tr} = \frac{\mathbb{F}S^k_{1-\alpha}[jC^{k_u}_\alpha - S^{k_u}_\alpha Z] + C^k_{1-\alpha}[C^{k_u}_\alpha Z + jS^{k_u}_\alpha]}{\mathbb{F}C^k_{1-\alpha}[jS^{k_u}_\alpha Z + C^{k_u}_\alpha] + S^k_{1-\alpha}[jC^{k_u}_\alpha Z - S^{k_u}_\alpha]} \tag{2.2}$$

where $\mathbb{F} = \frac{\rho^0 c^0}{\rho^0_u c^0_u}(1 + n_i e^{j\omega\tau_i})$ and notations for sine and cosine functions are $C^{k_u}_\alpha = cos(\alpha k_u L_i)$, $S^{k_u}_\alpha = sin(\alpha k_u L_i)$, $C^k_{1-\alpha} = cos((1-\alpha)kL_i)$, $S^k_{1-\alpha} = sin((1-\alpha)kL_i)$ and wavenumbers are $k = \omega/c^0$ and $k_u = \omega/c^0_u$. **Note that the $n-\tau$ model can be replaced by more complex flame descriptions such as Flame Describing Functions (Noiray *et al.* 2008) or transfer matrices (Polifke *et al.* 2001).**

The jump conditions at the burner/chamber junction at null Mach number read (Dowling 1995; Davies 1988; Poinsot & Veynante 2011):

$$p'_{i+\frac{1}{2}} = p'_{i+1} = p'_{b,i}(z = L_i) \tag{2.3}$$

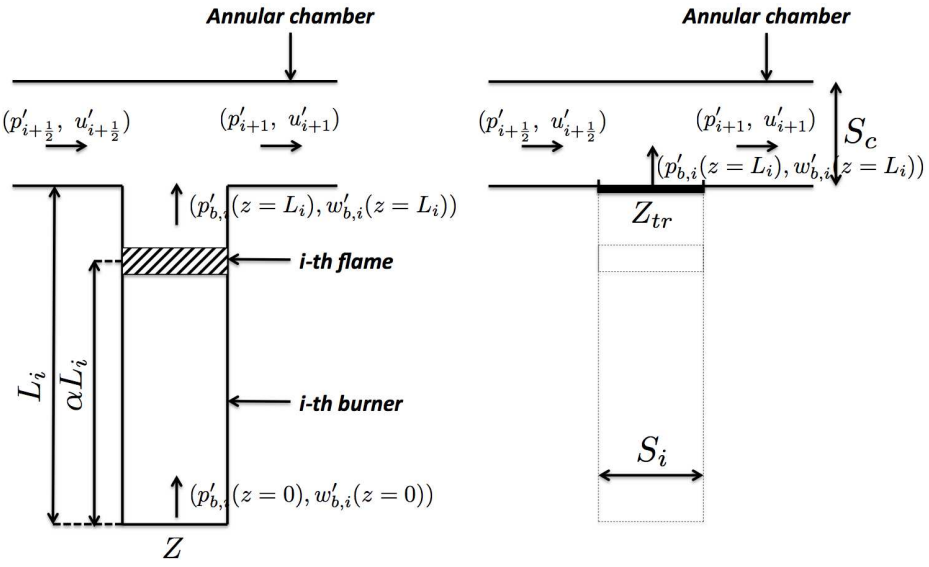

FIGURE 6. Equivalent impedance of the whole i^{th} burner (which includes the i^{th} active flame) near the burner/chamber interaction zone (figure 5). The translated impedance Z_{tr} at $z = L_i$ takes into account the upstream impedance Z at $z = 0$, the propagation in the cold ($0 < z < \alpha L_i$) and hot ($\alpha L_i < z < L_i$) parts of the burner as well as the active flame effect via the Flame Transfer Function ($n_i,\ \tau_i$)

$$u'_{i+\frac{1}{2}} S_c + \underbrace{w'_{b,i}(z=L_i)}_{=\frac{p'_{i+\frac{1}{2}}}{\rho^0 c^0 Z_{tr}}} S_i = u'_{i+1} S_c \tag{2.4}$$

Consequently, a transfer matrix T_i^* for the interaction part of figure 5 can be deduced:

$$\begin{bmatrix} p' \\ \rho^0 c^0 u' \end{bmatrix}_{i+1} = \begin{bmatrix} T_i^* \end{bmatrix} \begin{bmatrix} p' \\ \rho^0 c^0 u' \end{bmatrix}_{i+\frac{1}{2}} = \begin{bmatrix} 1 & 0 \\ 2j\Gamma_i & 1 \end{bmatrix} \begin{bmatrix} p' \\ \rho^0 c^0 u' \end{bmatrix}_{i+\frac{1}{2}} \tag{2.5}$$

where the coupling parameter Γ_i (Parmentier *et al.* 2012; Bauerheim *et al.* 2014*b*; Palies 2010; Schuller *et al.* 2012) (figure 5, burner/chamber interaction) is directly linked to the equivalent admittance $1/Z_{tr}$ of the whole i^{th} burner:

$$\Gamma_i = -\frac{j}{2}\frac{S_i}{S_c Z_{tr}} \tag{2.6}$$

When a velocity node ($Z = \infty$) or a pressure node ($Z = 0$) is imposed at the upstream end of each burner and flames are located at the burner/chamber junction ($\alpha = 1$), the coupling parameters Γ_i reduce to (using (2.2) and (2.6)):

$$\Gamma_i = \frac{1}{2}\frac{S_i \rho^0 c^0}{S_c \rho_u^0 c_u^0} tan(k_u L_i)\left(1 + n_i e^{j\omega\tau_i}\right) \text{ when } Z = \infty \tag{2.7}$$

$$\text{or } \Gamma_i = -\frac{1}{2}\frac{S_i \rho^0 c^0}{S_c \rho_u^0 c_u^0} cotan(k_u L_i)\left(1 + n_i e^{j\omega\tau_i}\right) \text{ when } Z = 0 \tag{2.8}$$

where $k_u = \frac{\omega}{c_u}$ and $(n_i,\ \tau_i)$ are the interaction index and the time-delay of the FTF for the i^{th} flame (Crocco 1951). **Note that the coupling term in equation (2.5) is $2j\Gamma_i p'_{i+\frac{1}{2}}$ thus burners and flames located at a pressure node have no effect**

on the acoustic mode, except in specific situations where Γ_i take infinite values. For instance, $\Gamma_i \to \infty$ in equation (2.8) when the burner length L_i goes to zero. It corresponds to the Blimbaum's exception case (Blimbaum *et al.* 2012) where the burner impedance attempts to force a pressure node at the burner/chamber junction. These specific situations require 3D acoustic considerations and are out of reach of this study: since $\Gamma_i \to \infty$, the low coupling factor assumption $\|\Gamma_i\| \ll 1$ (further described in equation (3.3)) is not satisfied meaning that no analytical solution can be provided.

Finally, equation (2.5) can be recast to relate characteristic waves $q^{\pm} = p' \pm \rho^0 c^0 u'$ instead of primitive variables p' and u' leading to the scattering matrix T_i:

$$\begin{bmatrix} q^+ \\ q^- \end{bmatrix}_{i+1} = \begin{bmatrix} T_i \end{bmatrix} \begin{bmatrix} q^+ \\ q^- \end{bmatrix}_{i+\frac{1}{2}} \text{ where } \begin{bmatrix} T_i \end{bmatrix} = \begin{bmatrix} 1+j\Gamma_i & j\Gamma_i \\ -j\Gamma_i & 1-j\Gamma_i \end{bmatrix} \tag{2.9}$$

The waves at both ends of the i^{th} sector are connected by the $M_i = T_i R_i$ scattering matrix using (2.1) and (2.9) (figure 5):

$$\begin{bmatrix} q^+ \\ q^- \end{bmatrix}_{i+1} = \begin{bmatrix} T_i \end{bmatrix} \begin{bmatrix} q^+ \\ q^- \end{bmatrix}_{i+\frac{1}{2}} = \underbrace{\begin{bmatrix} T_i \end{bmatrix} \begin{bmatrix} R_i \end{bmatrix}}_{M_i} \begin{bmatrix} q^+ \\ q^- \end{bmatrix}_{i} \tag{2.10}$$

Using the periodicity condition $\begin{bmatrix} q^+ \\ q^- \end{bmatrix}_{N+1} = \begin{bmatrix} q^+ \\ q^- \end{bmatrix}_{1}$ and equation (2.10) leads to:

$$\left(\prod_{i=N}^{1} M_i \right) \begin{bmatrix} q^+ \\ q^- \end{bmatrix}_{1} = \begin{bmatrix} q^+ \\ q^- \end{bmatrix}_{1} \tag{2.11}$$

The system defined by equation (2.11) has non-trivial solutions only if its determinant is null. Therefore, the ANR methodology provides an implicit analytical dispersion relation for the pulsation ω for a general non-symmetric BC configuration:

$$det \left(\prod_{i=N}^{1} M_i - I_d \right) = 0 \tag{2.12}$$

where I_d is the 2-by-2 identity matrix.

3. Analytical calculation of eigenfrequencies and mode structures

The analytical dispersion relation (equation 2.12) provides the frequencies and the structure of the modes of the annular chamber. It allows to study symmetry breaking by investigating the effects of the N burners responses (modelled by the N parameters $\Gamma_i,\ i \in [1, N]$ defined by equation (2.6)) on the growth rate and the nature of azimuthal modes. Several configurations are considered here (figure 7) to understand the effect of symmetry breaking on combustion instabilities.

3.1. *Unperturbed annular cavity (without burners and flames)*

First, an annular chamber with no burner (i.e. $\Gamma_i = 0$, for all $i \in [1, N]$) is studied as a reference case (figure 7, top left). The sound speed field corresponds to a reactive case: $c = c^0$ in the annular chamber. The transfer matrix of each sector (equation (2.10)) reduces to $M_i = R_i$ since $T_i = I_d$: only azimuthal propagation occurs. Consequently

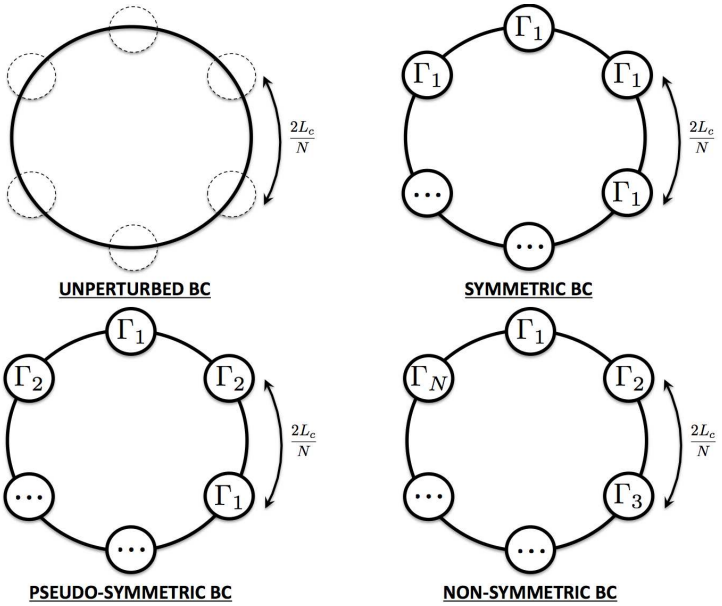

FIGURE 7. Typical configurations: Unperturbed (top left), symmetric with identical burners (top right), pseudo-symmetric configuration (bottom left) and the general non-symmetric configuration (bottom right)

equation (2.11) reduces to:

$$\begin{bmatrix} W^N & 0 \\ 0 & \frac{1}{W^N} \end{bmatrix} \begin{bmatrix} q^+ \\ q^- \end{bmatrix}_1 = \begin{bmatrix} q^+ \\ q^- \end{bmatrix}_1 \tag{3.1}$$

The dispersion relation is therefore $W^N = 1$ where $W = e^{2jkL_c/N}$. The N solutions of equation (3.1) are $W_0 = e^{2jp\pi/N}$ and correspond to real eigenfrequencies of the unperturbed problem:

$$kL_c = p\pi \quad \text{so that} \quad f = \frac{pc^0}{2L_c}, \text{ for all } p \in \mathbb{N} \tag{3.2}$$

As expected, equation (3.2) corresponds to a family of azimuthal modes where the first one ($p = 1$) is the first azimuthal mode at frequency $c^0/2L_c$ which is the mode observed in many practical cases. Equation (3.1) also provides the eigenvectors V associated to the eigenfrequencies f given by equation (3.2). In this situation, the generated eigenspace $\{V\}$ is two-dimensional: all azimuthal modes are degenerate and can be either standing, spinning or mixed. All modes are neutral since no acoustic dissipation is included (zero growth rate: $Im(f) = 0$).

3.2. *Non-symmetric BC configuration with active flames in the low-coupling limit*

Using a combustor with non-identical burners is a promising approach for controlling azimuthal modes (figure 7, bottom right). An asymptotic expansion of the dispersion relation (equation (2.12)) can be used to study this case. Since all burners can be different, all coupling parameters Γ_i (equation (2.6)) can be different. A fully analytical solution can be formulated when the solution is "close" to the unperturbed annular cavity case of Section 3.1. This is obtained by assuming small coupling parameters Γ_i:

$$\Gamma_i \ll 1, \text{ for all } i \in [1, N] \tag{3.3}$$

Under this assumption, a Taylor expansion of the transfer matrix of the whole system ($M = \prod_{i=N}^{1} T_i R_i$) at second order gives†:

$$M = \begin{bmatrix} W^N[1 + j\Sigma - Q(1)] + Q(W) + o(\Gamma_i^2) & j\sum_{i=1}^{N} \Gamma_i \left(\frac{1}{W}\right)^{N-2i+2} + o(\Gamma_i) \\ -j\sum_{i=1}^{N} \Gamma_i W^{N-2i+2} + o(\Gamma_i) & \frac{1}{W^N}[1 - j\Sigma - Q(1)] + Q(\frac{1}{W}) + o(\Gamma_i^2) \end{bmatrix} \tag{3.4}$$

where

$$\begin{cases} \Sigma = \sum_{i=1}^{N} \Gamma_i \\ Q(x) = \sum_{i=1}^{N-1} \sum_{j=i+1}^{N} \Gamma_i \Gamma_j x^{N-2(j-i)} \end{cases} \tag{3.5}$$

and the Landau notation $o(x)$ called "little-o" is used to designate any quantity negligible compared to x.

From equation (3.4), the dispersion relation at second order is:

$$\begin{aligned} det\,(M - Id) \approx & -\frac{W^{2N} - 2W^N + 1}{W^N} - \frac{j\Sigma(W^{2N} - 1)}{W^N} \\ & + \sum_{i=1}^{N-1} \sum_{j=i+1}^{N} \Gamma_i \Gamma_j [W^{2N} - W^{N-2(j-i)} - W^{2(j-i)} + 1] = 0 \end{aligned} \tag{3.6}$$

Equation (3.6) is a dispersion relation which involves terms ($W = e^{2jkL_c/N}$ and $\Gamma_i(k)$) depending on the wave number $k = \omega/c^0$. Under the low coupling assumption (equation (3.3)), the wavenumber k is close to the wavenumber of the unperturbed problem $k^0 = p\pi/L_c$ (Section 3.1): $k \approx k^0 + \epsilon/L_c$. A proper asymptotic expansion of $W^{\pm} = e^{2jkL_c/N} = e^{2j(p\pi+\epsilon^{\pm})/N} \approx e^{2jp\pi}(1 + 2j\epsilon^{\pm}/N)$ in terms of the wavenumber perturbations ϵ^+ and ϵ^- gives:‡

$$W^{\pm} = (1 + \mathcal{E}^{\pm})W_0 + o(\mathcal{E}^{\pm}) \;\text{ i.e. }\; kL_c = p\pi + \epsilon^{\pm} \;\text{ or }\; f^{\pm} = \frac{pc^0}{2L_c} + \frac{c^0}{2\pi L_c}\epsilon^{\pm} \tag{3.7}$$

where $W_0 = e^{2jp\pi/N}$ is the solution of the unperturbed problem and corresponds to $kL_c = p\pi$ (i.e. $f = \frac{pc^0}{2L_c}$) where p is the mode order, $\mathcal{E}^{\pm} = 2j\frac{\epsilon^{\pm}}{N}$ and $j^2 = -1$.

The coupling parameters Γ_i also depend on the frequency and therefore on $W^{\pm}$ (or $\epsilon^{\pm}$) and can be approximated by:

$$\Gamma_i(W) \approx \underbrace{\Gamma_i(W = W_0)}_{\Gamma_i^0} + \mathcal{E}^{\pm} W_0 \underbrace{\left(\frac{\partial \Gamma_i}{\partial W}\right)_{W=W_0}}_{\Gamma_i^1} \approx \Gamma_i^0 + \frac{2j\epsilon^{\pm} W_0}{N}\Gamma_i^1 \tag{3.8}$$

Using (3.7) and (3.8), a Taylor expansion of the terms $W(\epsilon^{\pm})$ and $\Gamma_i(\epsilon^{\pm})$ in the dispersion relation (3.6) at second order ($o(\epsilon^2)$ knowing that Γ_i^0 is of order of $\epsilon^{\pm}$)¶ gives:

$$A - 4B\epsilon^{\pm} + 4C{\epsilon^{\pm}}^2 = 0 \tag{3.9}$$

† A first-order Taylor expansion of extra-diagonal terms which have no zero order term is sufficient to compute a second-order dispersion relation of $det(M - Id)$.

‡ The two components V^+ and V^- of the azimuthal mode do not necessarily have the same wavenumber perturbation $\epsilon^{\pm}$. Therefore the notation $W^{\pm}$ is used since the azimuthal propagation of waves W depends on the wavenumber perturbation $\epsilon^{\pm}$.

¶ The analytical resolution of the dispersion relation will lead to the solution $\epsilon^{\pm} \propto \Gamma_i^0$ which proves that Γ_i^0 is a first order term and $\Gamma_i^0\Gamma_j^0$ or $\Gamma_i^0\epsilon^{\pm}$ are second order terms.

where

$$\begin{cases} A = -\left[W_0^{2N} - 2W_0^N + 1\right] - j\Sigma_0\left[W_0^{2N} - 1\right] \\ \qquad + \sum_{i=1}^{N-1}\sum_{j=i+1}^{N}\Gamma_i^0\Gamma_j^0\left[W_0^{2N} - W_0^{N-2(j-i)} - W_0^{2(j-i)} + 1\right] \\ B = \frac{j}{2}[W_0^{2N} - 1]\left[1 + \frac{\Sigma_1}{N}\right] - \frac{\Sigma_0}{2}[W_0^{2N} + 1] \\ C = \frac{1}{N^2}\left[\binom{N}{N-2}W_0^{2N} + \binom{N+1}{N-1}\right] \end{cases} \tag{3.10}$$

where $\Sigma_0 = \sum_{i=1}^{N}\Gamma_i^0$ and $\Sigma_1 = \sum_{i=1}^{N}\Gamma_i^1$, knowing that $\Gamma_i^{\pm}(\omega) \simeq \Gamma_i^0 + \frac{2j\epsilon^{\pm}}{N}W_0\Gamma_i^1$ (see equation (3.8)).

From Section 3.1, $W_0^N = 1$ which leads to simplifications of coefficients A, B and C:

$$\begin{cases} A = 4\displaystyle\sum_{i=1}^{N-1}\sum_{j=i+1}^{N}\Gamma_i^0\Gamma_j^0\left[\sin\left(\frac{2p\pi}{N}(j-i)\right)\right]^2 \\ B = -\Sigma_0 \\ C = 1 \end{cases} \tag{3.11}$$

Eigenfrequencies are deduced from the quadratic equation equation (3.9):

$$\epsilon^{\pm} = \frac{B \pm \sqrt{B^2 - AC}}{2C} \tag{3.12}$$

which leads to a simple expression for the wavenumber perturbations in the case of a general non-symmetric BC configuration:

$$\epsilon^{\pm} = -\frac{1}{2}\left(\Sigma_0 \pm \sqrt{\Sigma_0^2 - A}\right) \tag{3.13}$$

where $\Sigma_0 = \sum_{i=1}^{N}\Gamma_i^0$ will be called the "coupling strength" while A is the non-symmetric part defined in equation (3.11) depending on the number of burners N and the mode order p.

The term $\mathcal{S}_0 = \sqrt{\Sigma_0^2 - A}$ in equation (3.13) is called the "splitting strength" because it separates the two eigenvalues ϵ^+ and ϵ^-. It can be recast for simplification (see Appendix A) and highlights the key role of the $2p^{th}$ complex Fourier coefficients $\gamma(\pm 2p)$ of the azimuthal coupling factor distribution $\Gamma^0 = [\Gamma_1^0, ..., \Gamma_N^0]$:

$$\mathcal{S}_0^2 = \Sigma_0^2 - A = \sum_{i,j=1}^{N}\Gamma_i^0\Gamma_j^0 cos\left(\frac{4p\pi}{N}(j-i)\right) = \gamma(2p) \times \gamma(-2p) \tag{3.14}$$

where $\gamma(k) = \sum_{i=1}^{N}\Gamma_i^0 e^{-j2k\pi i/N}$ is the k^{th} Fourier coefficient of the coupling factor azimuthal distribution Γ^0.

Equation (3.13) is a generalization of Parmentier *et al.* (2012) and Noiray *et al.* (2011) results to an annular chamber connected by N burners with active flames. It shows that:

1) Stability of the N burners combustor is controlled to first order by the imaginary part of the coupling strength $\Sigma_0 = \sum_{i=1}^{N}\Gamma_i^0$. This coupling strength depends only on the sum of the individual coupling parameters Γ_i, not on the pattern used to distribute these burners when they differ.

2) The splitting strength $\mathcal{S}_0$ defined by equation (3.14) controls the nature of the modes: if $\mathcal{S}_0 = 0$ modes are degenerate (i.e. $\epsilon^+ = \epsilon^-$) and if $\mathcal{S}_0 \neq 0$, they are not.

Noiray *et al.* (2011) obtained a similar result where the mode was controlled by $\gamma_{HR}(2p)$, the $2p^{th}$ Fourier coefficient of the heat-release distribution. Equation (3.14) is a generalization of such a result: the present network model developed in this paper

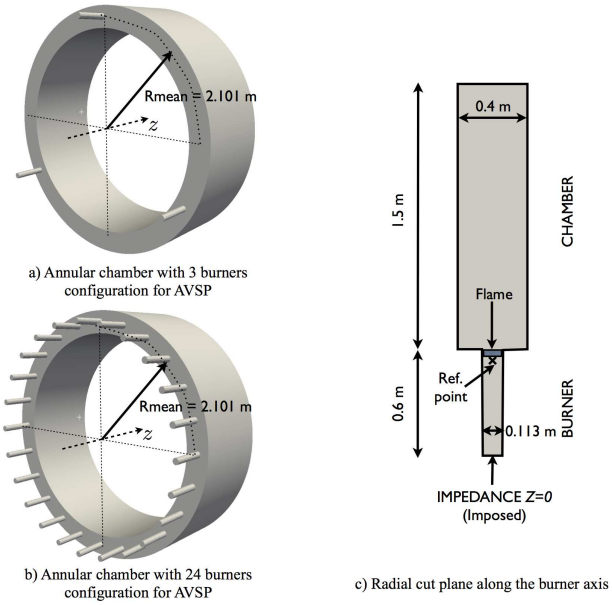

FIGURE 8. Toy-models to validate the ATACAMAC methodology. (a) Perfect annular chamber with $N = 3$, (b) $N = 24$ cylindrical burners, (c) burner/chamber configuration

shows that the mode is controlled by the azimuthal distribution of the coupling parameter Γ_i^0 which includes the active flame ($n-\tau$ model) but also by the geometry characteristics, the upstream impedance Z of the burners as well as the density and temperature differences between cold and burnt gases. All these features can affect the asymmetry of the system and therefore the stability: they cannot be neglected when studying combustion instabilities in annular chambers.

A summary of this analytical method providing the frequencies and the stability map of the p^{th} azimuthal mode in a chamber with N burners is given in Appendix B.

4. Application to a simplified multi-burner annular chamber

Analytical expressions of eigenfrequencies (equation (3.13)) of azimuthal modes are compared to results obtained with AVSP (Nicoud *et al.* 2007), a full 3D Helmholtz solver for two cases:

- A simplified academic configuration with $N = 3$ burners (Section 5).
- A realistic case with $N = 24$ burners (Section 6).

4.1. *Description of the configurations*

The 3D geometries correspond to a BC setup with $N = 3$ or $N = 24$ burners (figure 8) similar to figure 3 (physical and geometrical parameters are defined in table 1). The burner/chamber interfaces are placed at $z = 0$ and the flames are on the burner side. The flame width is equal to 2 mm which guarantees its compacity with respect to the acoustic wave length. Boundary conditions correspond to impermeable walls everywhere except at the upstream end of burners where an impedance $Z = 0$ (i.e. $p' = 0$) is imposed to mimic a connection to a large plenum. For the $N = 3$ burners configuration, two cases are investigated (table 2): first with identical burners and then with two types of burners with different time-delays τ_1 and τ_2. The interaction index of flames is set to the same

CHAMBER			
Half perimeter	L_c	6.59	m
Section	S_c	0.6	m^2
BURNER			
Number	N	3 or 24	$-$
Length	L_i^0	0.6	m
Section	S_i	0.01	m^2
FRESH GASES			
Mean temperature	T_u^0	700	K
Mean density	ρ_u^0	9.79	kg/m^3
Mean sound speed	c_u^0	743	m/s
BURNT GASES			
Mean temperature	T^0	1800	K
Mean density	ρ^0	3.81	kg/m^3
Mean sound speed	c^0	1191	m/s
FLAME PARAMETERS			
Interaction index	n_i	1.0	$-$
Time-delay	τ_i	*variable*	s

TABLE 1. Parameters used for numerical applications. They correspond to a typical large scale industrial gas turbine.

NAME	N	CBO	ASYMMETRY PATTERN
B3_C0	3	0	○ ○ ○
B3_C1	3	1	○ ● ○
B24_C0	24	0	○ ○
B24_C20_P1	24	20	● ● ● ● ● ● ● ● ● ○ ○ ○ ○ ● ● ● ● ● ● ● ● ● ●
B24_C20_P2	24	20	● ● ● ● ● ○ ● ● ● ● ○ ● ● ● ● ● ● ○ ● ● ● ● ● ○
B24_C20_P3	24	20	● ● ● ● ● ● ● ● ○ ○ ● ● ● ● ○ ○ ● ● ● ● ● ● ● ●
B24_C20_P4	24	20	● ● ● ● ● ○ ● ● ● ● ● ○ ● ● ● ● ● ○ ● ● ● ● ● ○
B24_C24	24	24	● ●

TABLE 2. BC configurations investigated with both the 3D Helmholtz solver AVSP and the analytical approach ATACAMAC. ○: Burner without CBO ●: Burner with CBO

value $n = 1.0$ (knowing that typical low-frequency values for n are around $\frac{T^0}{T_u^0} - 1 \simeq 1.57$ here (Poinsot & Veynante 2011)) in each burner.

For the $N = 24$ configuration (figure 8), two types of burners with different time-delays are mixed to mimic the combustion chamber where burners can be equipped (or not) with CBO's (Cylindrical Burner Outlet) to modify their flame response (Berenbrink & Hoffmann 2001; Krueger *et al.* 2000). Table 2 displays the circumferential patterns (● for CBO buners and ○ for burners without CBO) which are considered.

4.2. *Description of the 3D acoustic code*

Assumptions and results of ATACAMAC can be validated using a full 3D acoustic solver called AVSP (Nicoud *et al.* 2007; Silva *et al.* 2013; Selle *et al.* 2006; Sensiau *et al.* 2009) which solves the Helmholtz equation in a reactive flow without the assumptions used in ATACAMAC (Nicoud *et al.* 2007) but of course at a higher cost. AVSP takes into account the interaction between combustion and acoustics. It solves the eigenvalue problem issued from the discretization on unstructured meshes of the Helmholtz equation at zero Mach number. Meshes contain approximately 2 millions cells (corresponding to the ratio of the wavelength to the longest cell length $\lambda/\Delta h_{max} \simeq 250$) which is sufficient considering the simplicity of the geometry and the wavelength of the first azimuthal modee. Source terms due to flames are modeled using Flame Transfer Functions (FTF) (Crocco 1951). The local heat release fluctuations are expressed in the burner i as:

$$q'_i = n_{u,i}\, e^{j\omega\tau_i}\, \vec{u}'(\mathbf{x}_{ref,i}) \cdot \vec{n}_{ref,i}. \tag{4.1}$$

where $\mathbf{x}_{ref,i}$ is a reference point upstream of the flame in burner i.

The local interaction index $n_{u,i}$ describes the local flame-acoustic interactions. The values of $n_{u,i}$ are assumed to be constant in the flame zone i (figure 8) and are chosen to recover the global value of the interaction index n_i corresponding to the infinitely thin flame when integrated over the flame zone i (Nicoud *et al.* 2007). For the sake of simplicity, they are also assumed to be independent of frequency. These assumptions allow to use AVSP to check the precision of the analytical techniques developed in ATACAMAC.

In annular configurations with multiple burners, the heat release fluctuations in burner i are assumed to be driven by velocity fluctuations at the reference point $\mathbf{x_{ref,i}}$. This assumption, called ISAAC (Independence Sector Assumption in Annular Combustor) in (Sensiau *et al.* 2009) was validated by an LES of a full annular combustor (Staffelbach *et al.* 2009) and is used in the present study. In the infinitely thin flame model used in ATACAMAC the reference points are chosen at the flame locations $z_{f,i}$. The normalized abscissa of the flame is set to $\alpha \simeq 0.91$ (Bauerheim *et al.* 2014*b*). 3D effects near the burner/chamber junctions can be accounted for (Pierce 1981) using a standard length correction in the low-frequency range for a flanged tube (Silva *et al.* 2009) which is applied at the downstream burner's end ($\Delta L_i = 0.4\sqrt{4S_i/\pi}$). In AVSP, the reference points are placed a few millimeters upstream of the flames (figure 8) for numerical accuracy issues (Silva *et al.* 2013).

5. Symmetry breaking with $N = 3$ burners

Analytical expressions of frequency of azimuthal modes (equation (3.13)) can be obtained for a generic annular BC configuration with N burners. First, the symmetric case (figure 9, left) with $N = 3$ identical burners is studied (Section 5.1). Then, the effect of circumferential variations on combustion instabilities is investigated (Section 5.2) and validated on an asymmetric BC configuration where one type 1 burner is replaced by a type 2 (figure 9, right).

5.1. *Symmetric case with $N = 3$ identical burners*

In an axisymmetric configuration where burners are the same for all sectors (i.e. $\Gamma_i = \Gamma$, for all $i \in [1, 3]$), only two different mode types exist. Indeed, the splitting strength $\mathcal{S}_0$ in equation (3.14) simplifies depending on the mode order p and the number of burners N (Appendix A):

$$\begin{cases} \text{If } p = 3m, \text{ for } m \in \mathbb{N} \text{ then } \mathcal{S}_0 = 3\Gamma^0 \\ \text{For any other mode of order } p : \mathcal{S}_0 = 0 \end{cases} \tag{5.1}$$

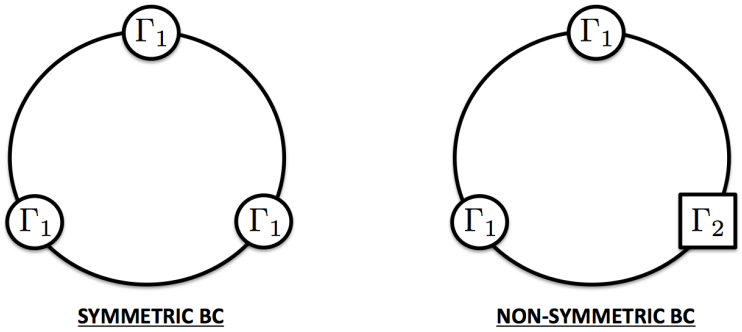

FIGURE 9. Schematic view of the BC configuration with $N = 3$ burners for the validation of numerical and analytical resolutions of equation (2.12). Left: symmetric case (all interactions terms Γ_i (equation (2.6)) are equal) ; Right: asymmetric case (two identical burners with the same Γ_1 and one burner with Γ_2)

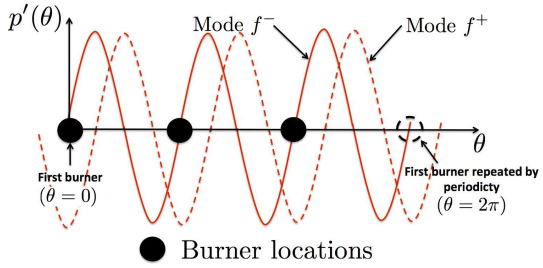

FIGURE 10. Pressure structure of the two components of the azimuthal mode in a $N = 3$ burners configuration: a standing mode imposing a pressure node at every burner locations (——— , f^-) and a standing mode imposing a pressure anti-node at every burner locations (- - - , f^+).

Consequently, only two different classes of modes can develop in annular BC configurations with $N = 3$ identical burners:

• **Non-degenerate singlets:** If $p = 3m,\ m \in \mathbb{N}$ the splitting strength is not null ($\mathcal{S}_0 = \Sigma_0 = 3\Gamma^0$, equation (3.14)) and the azimuthal mode is split into two components V^- and V^+ with different wavenumber perturbations ($\epsilon^\pm$) and frequencies ($f^\pm$) (equation (3.7)):

$$\left\{ \begin{array}{l} \epsilon^- = 0 \\ \epsilon^+ = -3\Gamma^0 \end{array} \right. \quad \text{corresponding to} \quad \left\{ \begin{array}{l} f^- = \frac{pc^0}{2L_c} \\ f^+ = \frac{pc^0}{2L_c} - \frac{3}{2}\frac{c^0\Gamma^0}{\pi L_c} \end{array} \right. \tag{5.2}$$

Figure 10 displays the mode structure associated to f^+ and f^-: due to symmetry considerations, these modes (e.g. p=3) can lock on burners ($N = 3$) (see Bauerheim *et al.* (2014*a*) for an analytical proof). Their wavelength corresponds to the chamber perimeter (or its half in a case of a configuration with an even number of burners). The first mode V^- with frequency f^- is standing and imposes a pressure node at every burner: therefore it is unperturbed by them ($\epsilon^- = 0$); the mode is neutral. The second mode V^+ at the frequency f^+ is also standing but imposing an azimuthal velocity node (i.e. a pressure anti-node) at every burner ($\epsilon^+ = -3\Gamma^0$).

• **Degenerate doublets:** All other azimuthal modes ($p \neq 3m,\ m \in \mathbb{N}$) are composed of two eigenmodes $V^\pm$ which have the same frequencies (degenerate modes) because the

splitting strength $\mathcal{S}_0 = 0$:

$$\left\{ \begin{array}{l} \epsilon^- = -\frac{3}{2}\Gamma^0 \\ \epsilon^+ = -\frac{3}{2}\Gamma^0 \end{array} \right. \text{ corresponding to } \left\{ \begin{array}{l} f^- = \frac{pc^0}{2L_c} - \frac{3}{4}\frac{c^0\Gamma^0}{\pi L_c} \\ f^+ = \frac{pc^0}{2L_c} - \frac{3}{4}\frac{c^0\Gamma^0}{\pi L_c} \end{array} \right. \tag{5.3}$$

In this configuration, the transfer matrix of the whole system (M defined in equation (3.4)) is equivalent to the null matrix. The mode nature is undetermined as pointed out by Noiray *et al.* (2011): a standing, spinning or mixed mode can develop. Noiray *et al.* (2011) have shown that non-linearities on the FTF can however promote one of these natures, a phenomenon which cannot be described by ATACAMAC since it is based on linear FTFs.

Figures 11 and 12 provide two validation points (marked by $\bullet$) of ATACAMAC for symmetric configurations using the full 3D acoustic solver AVSP: modes denoted $A^{\pm}$ when $\tau_1/\tau_c^0 = \tau_2/\tau_c^0 = 0.23$ and $E^{\pm}$ when $\tau_1/\tau_c^0 = \tau_2/\tau_c^0 = 0.68$. A good agreement is obtained between the acoustic code (AVSP) and ATACAMAC.

5.2. *Symmetry breaking with $N = 3$ different burners*

This section discusses the behavior of azimuthal modes when one of the three burners has a different FTF corresponding to a different value of Γ_i^0 (see figure 9, right). Especially, the observation in (Perrin & Charnley 1973; Sensiau *et al.* 2009) will be investigated: circumferential variations with specific patterns obtained by distributing different burner types along the azimuthal direction could split nominally degenerate doublets into non-degenerate singlets, as observed by Sensiau *et al.* (2009). If two burners have a coupling factor Γ_1^0 and the third one Γ_2^0, equation (3.13) can be solved with $N = 3$ and gives the following solution:

• **Non-degenerate singlets:** Azimuthal modes with $p = 3m,\ m \in \mathbb{N}$ are non-degenerate singlets characterized by $\mathcal{S}_0 = \Sigma_0 = 2\Gamma_1^0 + \Gamma_2^0$ (equation (3.14)) with wavenumber perturbations:

$$\left\{ \begin{array}{l} \epsilon^- = 0 \\ \epsilon^+ = -\Sigma_0 = -2\Gamma_1^0 - \Gamma_2^0 \end{array} \right. \text{ corresponding to } \left\{ \begin{array}{l} f^- = \frac{pc^0}{2L_c} \\ f^+ = \frac{pc^0}{2L_c} - \frac{c^0(2\Gamma_1^0+\Gamma_2^0)}{2\pi L_c} \end{array} \right. \tag{5.4}$$

where $\Sigma_0 = \sum_{i=1}^{N} \Gamma_i^0$. These modes, as in the symmetric cases, impose a pressure node or pressure anti-node at each burner location leading to two modes with different frequencies: $f^+ \neq f^-$.

• **Nearly degenerate singlets:** For other azimuthal modes ($p \neq 3m,\ m \in \mathbb{N}$), equation (3.13) leads to nearly degenerate singlets (Perrin & Charnley 1973): the degenerate doublet encountered in symmetric configurations (denoted DD with $\epsilon_{DD} = -\frac{1}{2}\Sigma_0 = -\Gamma_1^0 - \frac{1}{2}\Gamma_2^0$, equation (5.3)) is split depending on the splitting strength $\mathcal{S}_0 = \Gamma_1^0 - \Gamma_2^0$ (equation (3.14) for the $N = 3$ case with the pattern 121 ($\circ\bullet\circ$, table 2)):

$$\epsilon^{\pm} = \underbrace{-\frac{1}{2}\Sigma_0}_{\epsilon_{DD}} \ \pm \ \underbrace{\frac{1}{2}\mathcal{S}_0}_{\text{Splitting}} \tag{5.5}$$

$$\text{so that } \ \epsilon^- = -\frac{1}{2}\left(\Gamma_1^0 + 2\Gamma_2^0\right) \text{ and } \epsilon^+ = -\frac{3}{2}\Gamma_1^0 \tag{5.6}$$

These results were validated in figures 11 and 12 for the first azimuthal mode ($p = 1$) of the configuration $B3\_C1$ with the pattern 121 ($\circ\bullet\circ$, table 2) where coupling parameters are defined by equation (2.8).

When $\mathcal{S}_0 \neq 0$, the nominally doublet is split into two dissimilar azimuthal modes (e.g. modes denoted B^+ and B^- in figure 11 corresponding to $\tau_1/\tau_c^0 = 0.55$ and $\tau_2/\tau_c^0 = 0.23$)

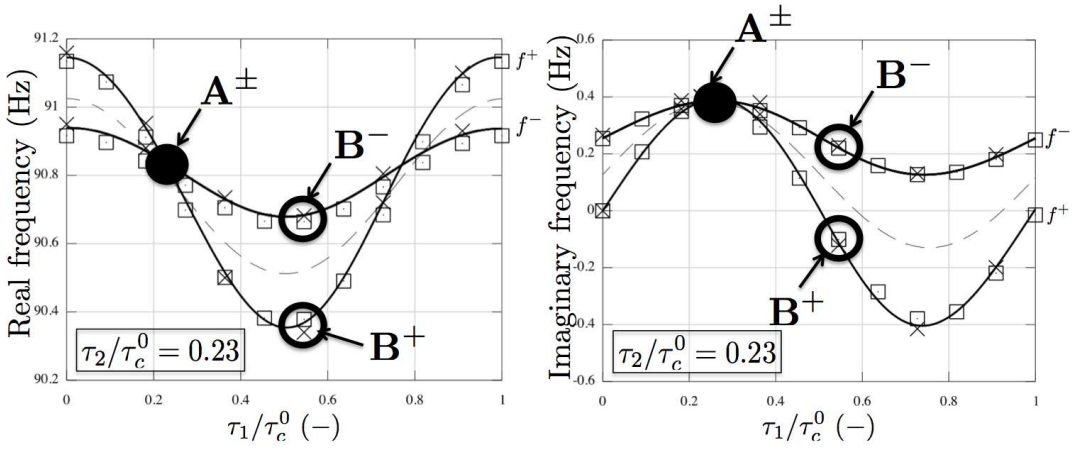

FIGURE 11. Real and imaginary part of the frequency f^+ and f^- of the two components of the first mode ($p = 1$) in the B3_C1 configuration with the pattern 121 ($\circ \bullet \circ$) and a fixed $\tau_2/\tau_c^0 = 0.23$. —— : Atacamac (numerical resolution of equation (2.12)), □: Atacamac (analytical formula equation (5.6)), ×: AVSP, - - - : Trajectory of the modes average $(f^+ + f^-)/2$, •: Symmetric case where $\tau_1/\tau_c^0 = \tau_2/\tau_c^0 = 0.23$, τ_c^0 corresponds to $\frac{1}{f_0} \simeq 11\ ms$.

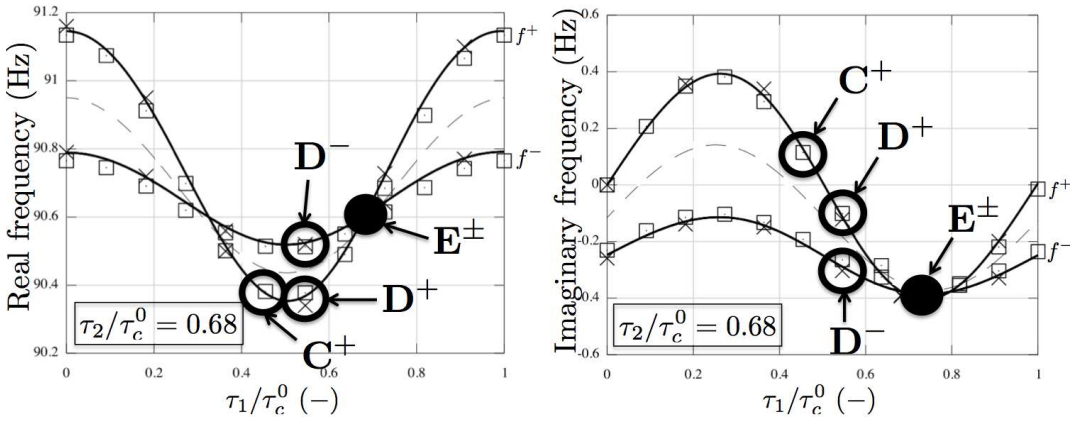

FIGURE 12. Real and imaginary part of the frequency f^+ and f^- of the two components of the first mode ($p = 1$) in the B3_C1 configuration with the pattern 121 ($\circ\bullet\circ$) and a fixed $\tau_2/\tau_c^0 = 68$. —— : Atacamac (numerical resolution of equation (2.12)), □: Atacamac (analytical formula equation (5.6)), ×: AVSP, - - - : Trajectory of the modes average $(f^+ + f^-)/2$, •: Symmetric case where $\tau_1/\tau_c^0 = \tau_2/\tau_c^0 = 0.68$, τ_c^0 corresponds to $\frac{1}{f_0} \simeq 11\ ms$.

with close frequencies and different growth rates as mentioned in (Perrin & Charnley 1973; Sensiau *et al.* 2009). The term $\mathcal{S}_0 = \Gamma_1^0 - \Gamma_2^0$ for the pattern 121 ($\circ \bullet \circ$) measures the differences in flame response between the two burner types and controls the degree of degeneracy of the azimuthal mode†.

Figure 13 displays the associated mode structure of the symmetric (mode A) and asymmetric (mode B) cases. For symmetric configurations, the mode structure is undetermined so that both spinning or standing modes can occur (figure 13, top). However,

† Note that some asymmetry could still give degenerate doublets (i.e. $\mathcal{S}_0 = 0$): for instance, the first order mode ($p = 1$) of a $N = 6$ burners BC configuration with the pattern ($\bullet \circ \bullet \circ \bullet \circ$) or ($\bullet \bullet \bullet \circ \circ \circ$) is a doublet with $\epsilon = -\frac{3}{2}(\Gamma_1^0 + \Gamma_2^0)$.

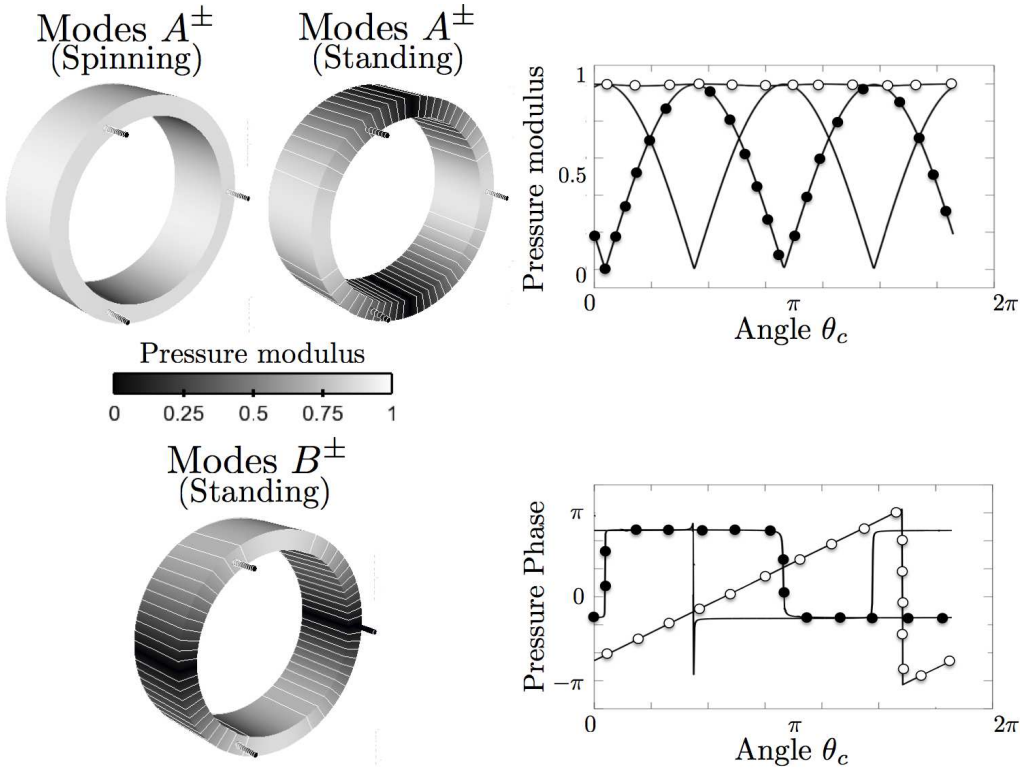

FIGURE 13. 3D and isolines of pressure modulus (left) and modulus and phase of acoustic pressure (right) of the first azimuthal modes ($p = 1$) of the asymmetric case B3_C1 with the pattern 121 ($\circ \bullet \circ$, table 2) in two situations: mode A ($\tau_1/\tau_c^0 = \tau_2/\tau_c^0 = 0.23$) and mode B ($\tau_1/\tau_c^0 = 0.55$ and $\tau_2/\tau_c^0 = 0.23$). $\circ$: $A^{\pm}$ (spinning), $\bullet$: $A^{\pm}$ (standing), ——— : $B^{\pm}$ (standing)

breaking the symmetry using two different burner types (e.g. mode B with $\tau_1/\tau_c^0 = 0.55$ and $\tau_2/\tau_c^0 = 0.23$) leads to standing modes only (figure 13, bottom).

5.3. *Conclusion on symmetry breaking in the $N = 3$ case*

Sections 5.1 and 5.2 show that the splitting strength $\mathcal{S}_0$ defined by equation (3.14) controls both the stability and the mode structure of an annular chamber ($N = 3$) where two types of burners are installed. Nevertheless, a "necessary condition" for stability can be derived independently of the splitting strength value. Indeed, the imaginary part of the modes average $\frac{1}{2}Im(\epsilon^+ + \epsilon^-)$ does not depend on the splitting strength $\mathcal{S}_0$ but only on the total coupling strength $\Sigma_0 = \sum_{i=1}^{N} \Gamma_i^0$ yielding a necessary condition for stability:

$$\frac{1}{2}I_m(\epsilon^+ + \epsilon^-) = -\frac{1}{2}I_m\left(\Sigma_0\right) < 0 \tag{5.7}$$

If this condition is not fulfilled (figure 14, left), there is no hope of stabilizing the mode since at least one of the two components of the azimuthal mode (V^+ or V^-) will remain unstable (e.g. $A^{\pm}$ and B^+ in figure 11).

For a symmetric case where the splitting strength $\mathcal{S}_0$ is zero, equation (5.7) is a necessary and sufficient condition to have a stable mode. However, when symmetry is broken,

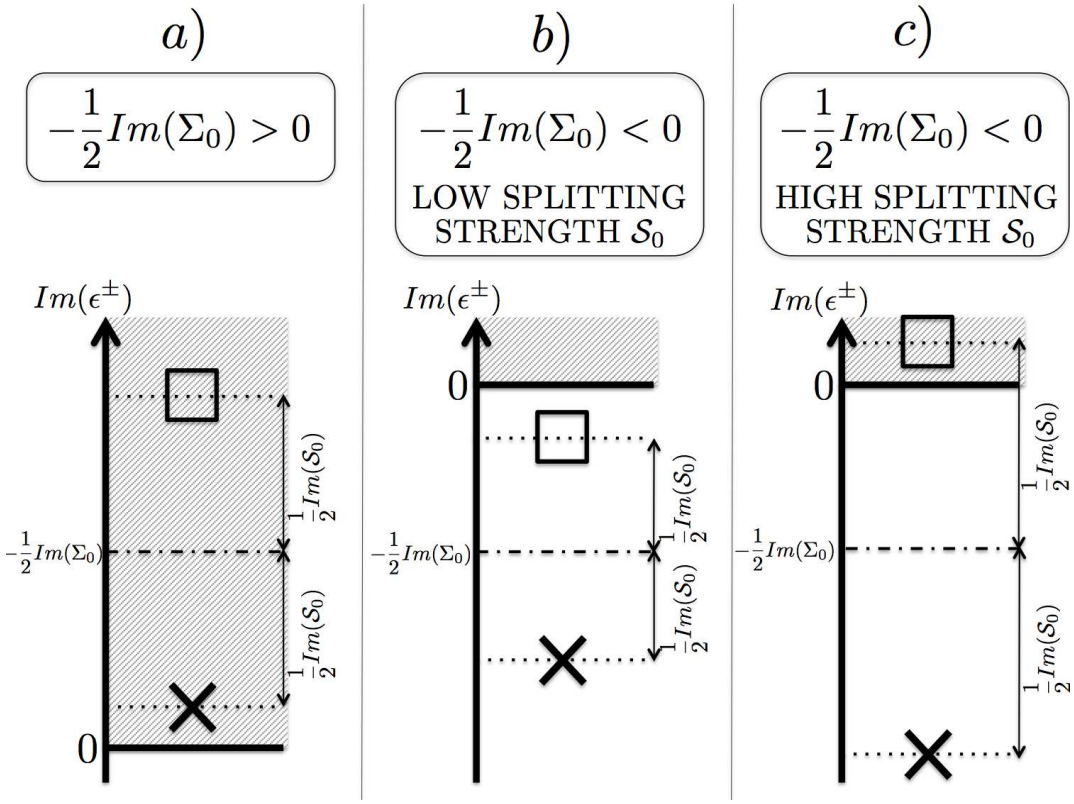

FIGURE 14. Mode stability for an annular chamber with N burners depending on the condition (5.7) and the splitting strength $\frac{1}{2}Im(\mathcal{S}_0)$. $\times$: ϵ^- and $\square$: ϵ^+. The splitting strength is $\mathcal{S}_0^2 = \sum_{i,j=1}^{N} \Gamma_i^0 \Gamma_j^0 cos\left(\frac{4p\pi}{N}(j-i)\right)$ (equation (3.14)) and measures the difference between the two burner types 1 and 2. Shaded areas correspond to unstable zones. a) All modes are unstable, b) all modes are stable and c) symmetry breaking makes one mode unstable: the splitting strength $\mathcal{S}_0$ must be reduced to stabilize both modes as in the situation b).

satisfying condition (5.7) cannot guarantee stability (figure 14, middle and right). In this case, the necessary and sufficient condition becomes†:

$$max(Im(\epsilon^+), Im(\epsilon^-)) < 0 \tag{5.8}$$

because the splitting introduced by symmetry breaking (measured by the splitting strength $\mathcal{S}_0$) has to be taken into account. For weak splitting (figure 14, middle) the two modes V^+ and V^- remain stable (e.g. eigenmodes $D^{\pm}$ in figure 12) but for higher splitting (figure 14, right) one mode can become unstable (e.g. mode C^+ in figure 12).

6. Symmetry breaking in a $N = 24$ burners BC configuration

Conclusions of Section 5.3 obtained with $N = 3$ burners suggest a strategy to stabilize the p^{th} mode of a general N burners configuration as described in figure 15. Axisymmetric configurations (left part of figure 15) only have one degree of freedom to stabilize the

† Note that $max(Im(\epsilon^+), Im(\epsilon^-)) > \frac{1}{2}I_m(\epsilon^+ + \epsilon^-)$ and for a symmetric configuration $\epsilon^+ = \epsilon^-$.

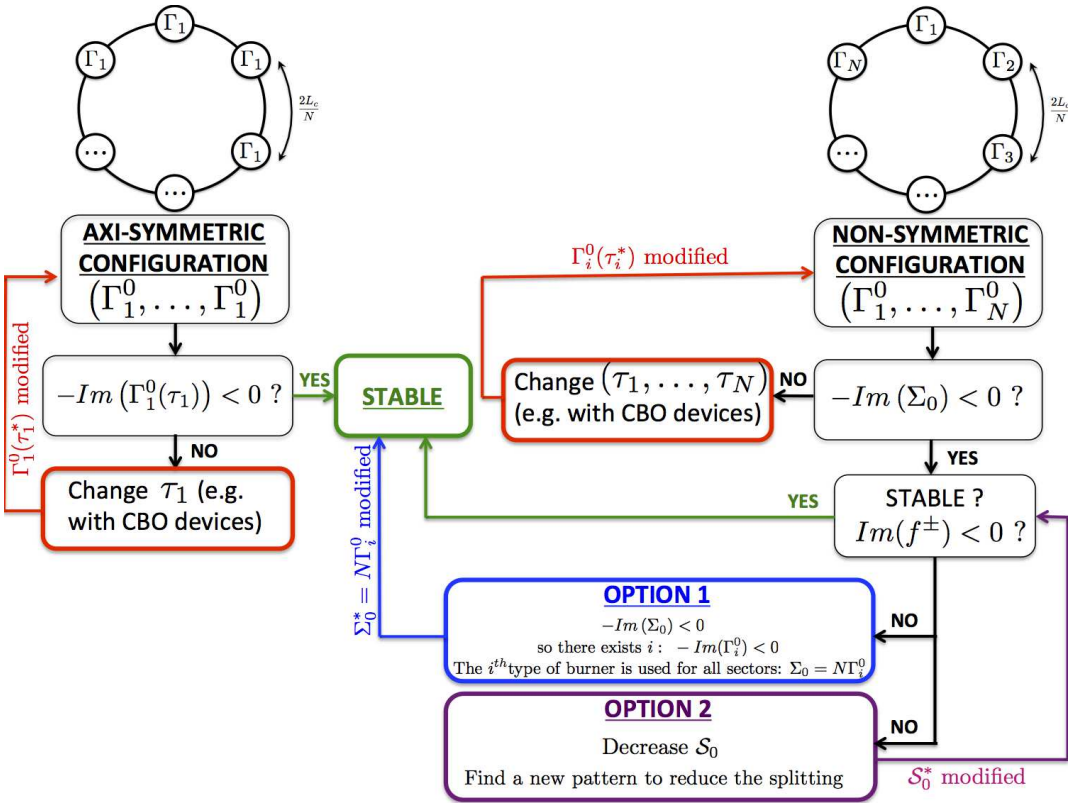

FIGURE 15. Strategy to stabilize an annular combustor.

p^{th} mode which is the time-delay τ_1: if τ_1 is such that condition (5.7) is met, then the configuration is stable.

For non-symmetric configurations (right part of figure 15), however, satisfying equation (5.7) does not guarantee the stabilization of the configuration. In this case, the asymmetry pattern is an additional degree of freedom and two options are available to ensure the stability of the p^{th} azimuthal mode:

- **Symmetrize the configuration (Option 1)**: if condition (5.7) is satisfied, at least one kind of injector satisfies $-Im(\Gamma_i^0) < 0$: this kind of burner can be used for all sectors which leads to the mode's stabilization. This option is the most efficient method to stabilize an azimuthal mode since no splitting occurs.
- **Reduce the asymmetry effect (Option 2)**: Another solution is to keep the same kind of burners $(\Gamma_1^0, ..., \Gamma_N^0)$ but rearrange them to reduce the splitting of the azimuthal mode and stabilize it. Optimization can be performed to find the best pattern which leads to the smallest value of the splitting strength $\mathcal{S}_0$.

As an example, symmetry breaking is studied here for a $N = 24$ burners configuration (Berenbrink & Hoffmann 2001; Krueger *et al.* 2000) representative of real industrial gas turbines. First, the stability of the first azimuthal mode ($p = 1$) of the symmetric configuration is studied as a function of the time-delay τ (which is the same for all burners), with the interaction index $n = 1.0$. Results (figure 16) show a very good agreement between the numerical and analytical solutions given by the 3D Helmholtz solver AVSP and ATACAMAC.

To break symmetry two different burners are then mixed, characterized by different

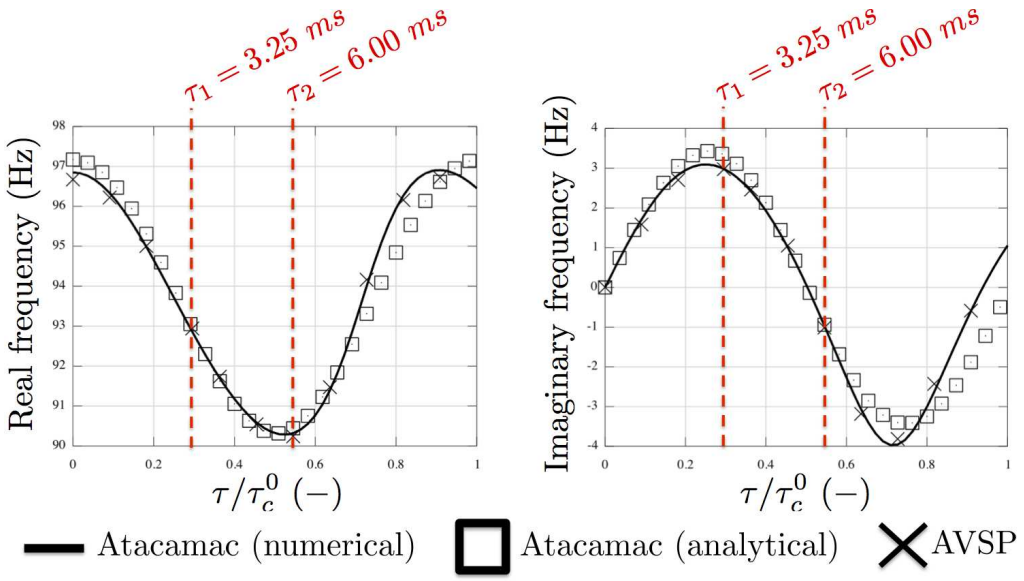

FIGURE 16. Stability map depending on τ of the first azimuthal mode ($p = 1$) of the symmetric BC configuration with 24 burners. τ_c^0 is the period of the first azimuthal mode $\tau_c^0 = 1/f^0 = \frac{2L_c}{pc^0} \simeq 11ms$

time-delays, τ_1 and τ_2 (figure 16). A time delay $\tau_1 = 3.25\ ms$ corresponds approximately to the most unstable burner ($Im(f_{AVSP}) = 2.98\ s^{-1}$, in figure 16 right), which is assimilated here to the baseline case, a burner without CBO ($\circ$ in table 2). CBOs (Cylindrical Burner Outlet) device can be mounted on some of the burners (Berenbrink & Hoffmann 2001; Krueger *et al.* 2000) to modify the flame time-delay and to stabilize the chamber. The length of the cylinder is such that the time lag τ_2 from the injection port to the flame front is increased by approximately a quarter of an acoustic period: $\tau_2 = \tau_1 + \frac{1}{4f^0} \simeq 6ms$ (since the first azimuthal mode has a frequency $f^0 \simeq 90Hz$): it corresponds to a stable burner where $Im(f_{AVSP}) = -1.01\ s^{-1}$ in figure 16 ($\bullet$ in table 2). Note that using 20 burners with $\tau_2 = 6\ ms$ and 4 burners with $\tau_1 = 3.25\ ms$ respects the necessary stability condition given by equation (5.7) (**---** for the configuration C_{20} in figure 17). The stability of the four patterns proposed in table 2 is studied using ATACAMAC and AVSP. Results are plotted in figure 17 (growth rates).

- **B24_C0:** This configuration corresponds to the unstable baseline case: the necessary condition (equation (5.7)) is not satisfied. Some burners have to be changed in order to get a stable combustor.
- **B24_C20_P1:** 20 CBOs devices have been mounted to try to stabilize the mode. The necessary condition (equation (5.7)) is satisfied. However this pattern has a large splitting strength $\mathcal{S}_0$. Consequently it splits azimuthal modes into two singlets with different growth rates making the first azimuthal mode unstable. This case is an excellent example of how, for asymmetric circumferential patterns, one can use stable burners that match the condition $-\frac{1}{2}I_m(\Sigma_0) < 0$ and yet, due to the asymmetry term $\mathcal{S}_0$, have an unstable mode as shown in figure 14 (right).
- **B24_C20_P2:** As suggested by figure 15, a solution to stabilize the mode is to find asymmetry patterns like $B24\_C20\_P2$ with a lower splitting strength $\mathcal{S}_0$ for which both singlets remain stable as mentioned in figure 14 (middle image).
- **B24_C20_P3 and B24_C20_P4:** The pattern $B24\_C20\_P2$ induces a low split-

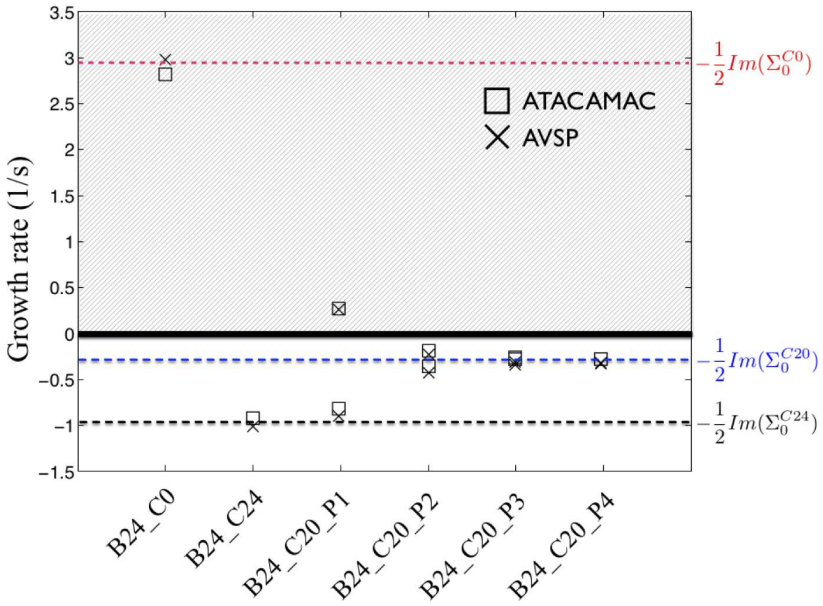

FIGURE 17. Growth rate of the first azimuthal mode ($p = 1$) for various asymmetry combination of burners with and without CBO: B24_C0 (24 noCBO burner), B24_C24 (24 CBO burners) and the four patterns B24_C20 (see table 2). `---` : Imaginary part of the modes average $-\frac{1}{2}I_m\,(\Sigma_0)$ depending on the configuration (C_0, C_{20} and C_{24})

ting strength and stabilizes the mode. However, optimal asymmetry patterns can be found which lead to no or very low splitting and therefore ensure the mode stabilization. Patterns $B24\_C20\_P3$ and $B24\_C20\_P4$ give stable degenerate doublets. In these cases, $\mathcal{S}_0 = 0$ and therefore equation (5.7) becomes a necessary and sufficient condition for stability. The mode is stable: $Im(f^{\pm}) \simeq -0.25\ s^{-1}$

- **B24_C24:** As explained in figure 15, the most efficient option to stabilize a mode is to symmetrize the annular combustor with burners which all satisfy the necessary condition (equation (5.7)), i.e. 24 burners with a CBO. The mode is very stable: $Im(f^{\pm}) \simeq -1.0\ s^{-1}$ (figure 17).

Considering the average imaginary part of the modes $-\frac{1}{2}Im(\Sigma_0)$ (`---` in figure 17), it is interesting to notice that, independently of the asymmetry patterns, combining 20 CBOs and 4 noCBOs burners give potentially less stable modes than using 24 CBOs: breaking symmetry has a limited interest here compared to adding CBOs on all burners. Nevertheless, if for any reason (ignition, pollution, construction, etc.) one must keep the two types of burner, the present analytical model offers an easy way to optimize the circumferential distribution of the burners by minimizing the imaginary part of the splitting strength $Im(\mathcal{S}_0)$. To illustrate this idea, figure 18 displays the effect of several asymmetry patterns on the splitting strength ($\mathcal{S}_0$) using a configuration with 20 CB0 - 4 noCBO burners. Appendix A shows that using two kinds of burners (with coupling parameters Γ_1^0 and Γ_2^0 respectively) yields a splitting strength of the form:

$$\mathcal{S}_0 = \overbrace{2\mathcal{K}}^{\text{Imposed by the pattern}} \underbrace{\left(\Gamma_1^0 - \Gamma_2^0\right)}_{\text{Imposed by the difference between burner types 1 and 2}} \tag{6.1}$$

where the reduced splitting strength $\mathcal{K}$ depends only on the asymmetry pattern (see

NAME	ASYMMETRY PATTERN	$\mathcal{K}$
P1	●●●●●●●●●●○○○○●●●●●●●●●●	$\frac{1}{2}\sqrt{3\sqrt{3}+6} \simeq 1.67$
P2	●●●●●○●●●●○●●●●●●○●●●●●○	$\frac{1}{2}\sqrt{2-\sqrt{3}} \simeq 0.26$
P3	●●●●●●●●○○●●●●○○●●●●●●●●	0
P4	●●●●●○●●●●●○●●●●●○●●●●●○	0

TABLE 3. Analytical expressions of the reduced splitting strength $\mathcal{K}$ for the four patterns described in Tab. 2

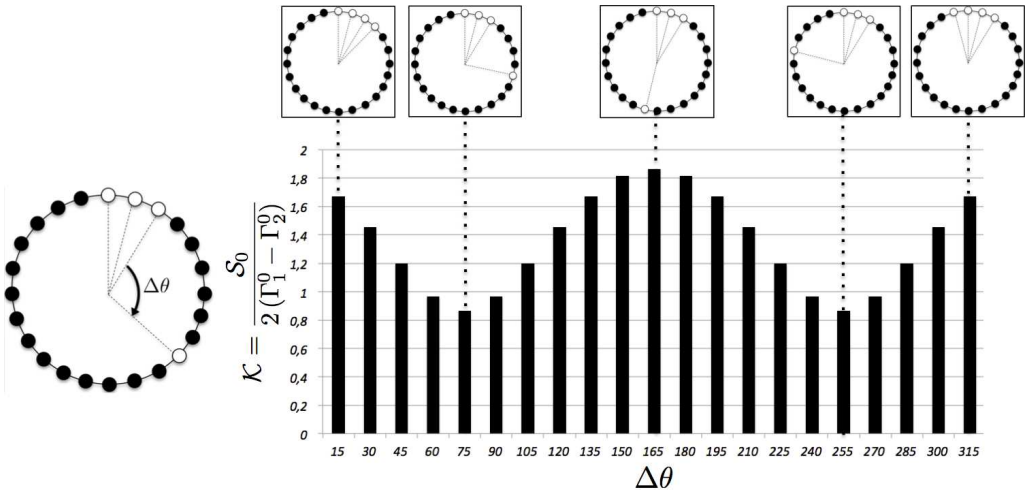

FIGURE 18. The reduced splitting strength ($\mathcal{K}$) for several patterns where three noCBO burners are kept together at the same place and the last noCBO burner's place is changed azimuthally. The splitting is then moderatly affected by the asymmetry pattern.

table 3 for the analytical expression of $\mathcal{K}$ for the four patterns studied). In equation (6.1), Γ_1^0 and Γ_2^0 are fixed by the burner characteristics so that minimizing $\mathcal{S}_0$ to increase stability is equivalent to minimizing $\mathcal{K}$.

Consequently, an optimization process appears as a promising approach to find patterns with the minimal value of the reduced splitting strength $\mathcal{K}$. This also highlights the potential of low-order models to perform optimization processes of large problems (here about 1,800 patterns are possible†) at very-low cost.

Finally, enumeration and distributions of reduced splitting strengths $\mathcal{K}$ (obtained numerically using (3.14) and (6.1) for the first azimuthal mode $p = 1$) are displayed in figure 19 depending on N_{noCBO}, the number of noCBO burner types ($N_{noCBO} = 2$, 4 and 6): all possible asymmetry patterns are computed where N_{noCBO} burners are chosen as burners without CBO while the $N - N_{noCBO}$ other ones correspond to burners with a CBO. The first burner of the pattern is always without CBO to avoid circular similarities. Figure 19 shows that more numerous and higher reduced splitting strength values are obtained when the number of noCBO burners (N_{noCBO}) is increased: these

† The problem addressed here corresponds to 4 no-CBO burners mixed with 20 CBO burners. When the first burner is fixed as a no-CBO type, the number of patterns is: $\binom{23}{3} = \frac{23!}{20! \times 3!} = 1,771$.

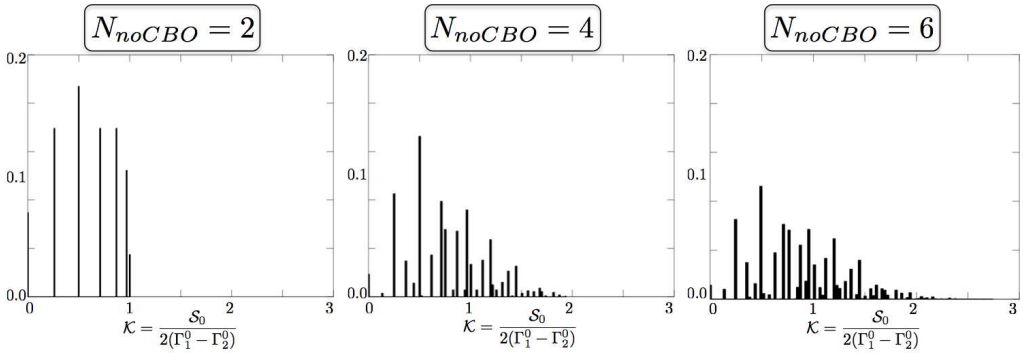

FIGURE 19. Distribution of the reduced splitting strength $\mathcal{K}$ vs. N_{noCBO}, the number of burners without CBO. All possible asymmetry patterns are used to compute each distribution: 23 patterns for $N_{noCBO} = 2$; 2275 for $N_{noCBO} = 4$ and 77804 for $N_{noCBO} = 6$).

situations are more complex to analyze and optimize. Moreover, only a few patterns lead to a small splitting strength.

Symmetry breaking can also modify the dynamic nature of the acoustic modes. The modulus and phase of acoustic pressure of the first azimuthal mode ($p = 1$) † are plotted in figure 20 for the four studied patterns (table 2), showing two distinct behaviors.

• **Patterns P1 and P2:** Patterns P1 and P2 give non-degenerate doublets: the two components V^+ and V^- of the azimuthal mode are standing (• in figure 20) and oscillate in opposite phase with different (yet very close) frequencies (e.g. 90.3 Hz and 91.3 Hz for the pattern P1). Figure 17 shows that for pattern P1, one mode is amplified whereas the other one is damped, resulting in an unstable standing mode.

• **Patterns P3 and P4:** On the other hand, asymmetry patterns leading to degenerate doublets have an undetermined mode structure: the two components V^+ and V^- of the azimuthal modes have the same frequencies so that they can be combined to obtain either a spinning (—— in figure 20), a standing (• in figure 20) or a mixed mode.

7. Conclusion

The present work describes a fully analytical approach, completed by a 3D numerical validation, to study the stability of azimuthal thermoacoustic modes in annular chambers. The analytical model is based on a quasi-one-dimensional zero-Mach number natural formulation where N burners are connected to a downstream annular chamber. Flames are supposed to be compact and are modeled using a Flame Transfer Function, characterized by a coupling factor and a phase shift. Manipulation of the corresponding acoustic equations yields a simple dispersion relation which can be solved analytically in specific situations where coupling factors are small (weak coupling). This analytical approach allows to predict the stability of azimuthal modes in symmetric cases where all burners are identical but also to study cases where different burner types are mixed in a chamber, using a predefinite pattern. The analytical method highlights the importance of two parameters:

• A "coupling strength" Σ_0 which is the sum of the individual coupling factors Γ_i^0 of each burner and controls the stability at first order.

• A "splitting strength" $\mathcal{S}_0$ defined in equation(3.14) which affects the stability and

† Only one of the two components of a given azimuthal mode is shown in figure 20.

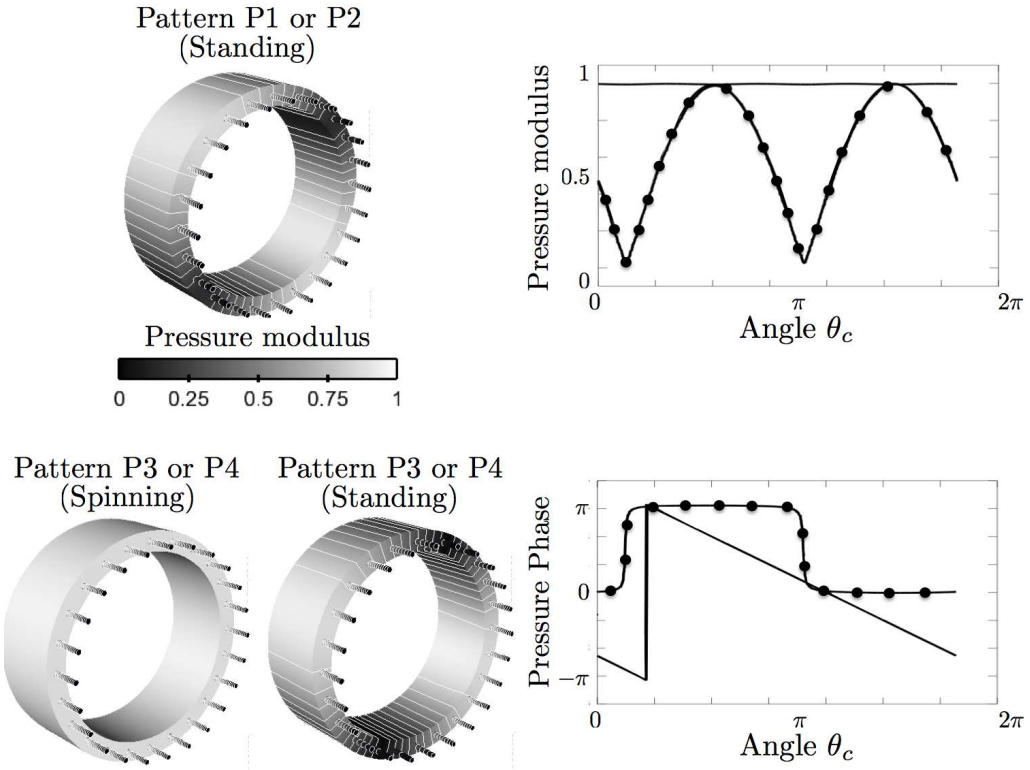

FIGURE 20. Effect of the asymmetry pattern on the azimuthal mode nature. 3D and isolines of the pressure modulus (left) and modulus and phase of the acoustic pressure over the circumference (right). P1 or P3: necessarily standing (•) ; P3 or P4: any combination of standing (•) or spinning(——).

the mode structure and depends on a combination of the coupling parameters of each burner.

First, a symmetric configuration with N identical burners with null inlet impedances (i.e. $p' = 0$) is studied. Only two mode behaviors are observed: degenerate doublets and non-degenerate singlets, the latter being capable of generating warbles (low frequency oscillations due to a non-degenerate mode (Perrin & Charnley 1973)). Then, a non-symmetric case where two different types of burners are distributed in the chamber is studied: symmetry breaking is proved to modify the azimuthal modes behavior in a simple case with only three burners in an annular chamber. The staging patterns can split nominally degenerate azimuthal modes (doublets) into non-degenerate pairs (singlets), a situation already mentioned in the literature and observed in recent Helmholtz simulations (Sensiau *et al.* 2009).

Finally, the effect of the asymmetry pattern is investigated in a $N = 24$ burners case representative of industrial gas turbines. A very good agreement is found for all cases between analytical and numerical results, obtained with a 3D Helmholtz solver. Results are compared to experimental observations where CBOs (Cylindrical Burner Outlet) are added to certain burners to control combustion instabilities. A simple criterion is derived to provide a necessary condition to stabilize an annular combustor. Since the asymmetry pattern does not appear in this criterion and the splitting strength is the only control parameter, this shows that symmetry breaking can modify the mode nature but has no real impact on mitigating combustion instabilities in annular chambers. The best

method to control a chamber with $N = 24$ sectors is to use 24 identical burners with FTF leading to stable azimuthal modes. However if keeping only one type of burner is not possible, a strategy to stabilize the mode is proposed: find an optimal pattern which leads to a low splitting of the corresponding azimuthal mode. The general character of this conclusion (a summary of this method is provided in Appendix B: this summary allows the computation of the "coupling strength", the "splitting strength", the frequency and the growth rate of all modes as soon as the FTF of each burner is known) is limited by the low coupling assumption which implies no interaction between burners. Strongly coupled situations where burners interfere (Bauerheim *et al.* 2014*b*; Worth & Dawson 2013*b*) may lead to an effect of the asymmetry pattern on the overall stabilization of the annular engines.

Appendix A. Analytical expression of the splitting strength

The general analytical expression of the splitting strength $\mathcal{S}_0$ is:

$$\mathcal{S}_0^2 = \sum_{i,k=1}^{N} \Gamma_i^0 \Gamma_k^0 \cos\left(\frac{4p\pi}{N}[k-i]\right) \tag{A 1}$$

Using $\cos(a-b) = \cos(a)\cos(b) + \sin(a)\sin(b)$ one may recast the splitting strength as:

$$\mathcal{S}_0^2 = \left[\sum_{i=1}^{N} \Gamma_i^0 \cos(4p\pi i/N)\right]^2 + \left[\sum_{i=1}^{N} \Gamma_i^0 \sin(4p\pi i/N)\right]^2$$

The above equation can be recast using the identity $a^2+b^2 = (a+jb)(a-jb)$ where $j^2=-1$:

$$\mathcal{S}_0^2 = \left[\sum_{i=1}^{N} \Gamma_i^0 e^{j4p\pi i/N}\right] \times \left[\sum_{i=1}^{N} \Gamma_i^0 e^{-j4p\pi i/N}\right] = \gamma(-2p) \times \gamma(2p) \tag{A 2}$$

where $\gamma(k)$ is the k^{th} Fourier coefficient of the asymmetry pattern Γ^0 defined as $\gamma(k) = \sum_{i=1}^{N} \Gamma_i^0 e^{-j2\pi ki/N}$.

Finally, the splitting strength is:

$$\mathcal{S}_0 = \sqrt{\gamma(2p) \times \gamma(-2p)} \tag{A 3}$$

The splitting strength obtained in the previous equation (A 3) gives some useful results:

• **1)** Noiray *et al.* (2011) obtained a similar result where the splitting strength is controlled only by $\gamma_{HR}(2p)$, the $2p^{th}$ Fourier coefficient of the heat-release distribution. Equation (A 3) is a generalization of such a result: the network model developed in this paper retains more geometry and flow features than the simple annular rig considered in (Noiray *et al.* 2011). In particular, it is shown here that the mode is controlled by the azimuthal distribution of the coupling parameter (which includes the active flame ($n-\tau$ model) but also the geometry characteristics, the upstream impedance Z of the burners as well as the difference between cold and burnt gases). It appears that all these features can effect the whole asymmetry of the system and therefore the stability and, consequently, cannot be neglected when studying combustion instabilities.

• **2)** If all coupling factors are the same (symmetric configuration), then the spectrum $\gamma(k)$ is null everywhere except for $k=0$ or $k=N$ (where $\gamma(0) = \gamma(N) = \Sigma^0 = \sum_{i=1}^{N} \Gamma_i^0$ is the total coupling of the system) which leads to two types of azimuthal modes:

a) If p is not $N/2$, N, $3N/2$ etc. then $\gamma(\pm 2p) = 0$ and the splitting strength is null:

$$\mathcal{S}_0 = 0 \tag{A 4}$$

These modes are characterized by no splitting: the two components of the azimuthal mode have the same frequencies and growth rates. They are called "degenerate doublets".

b) However, if $p = N/2$, N, $3N/2$ etc. then $\gamma(\pm 2p) = \sum_{i=1}^{N} \Gamma_i^0 = N\Gamma^0$ which gives:

$$\mathcal{S}_0 = N\Gamma^0 \tag{A 5}$$

These modes are characterized by a strong splitting: the two components of the azimuthal mode have different frequencies and growth rates. They are called "non-degenerate singlets".

• **3)** If only two types of burner are introduced in the combustion chamber (i.e. coupling factors can only take the value Γ_1^0 or Γ_2^0 for $i \in [1, N]$), then for mode satisfying $p \neq N/2, N, ...$ the splitting strength $\mathcal{S}_0$ can be decomposed as:

$$\mathcal{S}_0 = \overbrace{2\mathcal{K}}^{\text{Imposed by the pattern}} \underbrace{\left(\Gamma_1^0 - \Gamma_2^0\right)}_{\text{Imposed by the difference between burner types 1 and 2}} \tag{A 6}$$

where the reduced splitting strength $\mathcal{K}$ depends only on the asymmetry pattern and $(\Gamma_1^0 - \Gamma_2^0)$ is fixed by the burner characteristics.

Proof 1. *The Fourier coefficient $\gamma(k)$ can be viewed as a polynomial of degree one with N indeterminates (or variables) Γ_i^0 and coefficients depending on the asymmetry pattern. When considering only two burner types (corresponding to coupling factors Γ_1^0 and Γ_2^0), $\gamma(k)$ reduces to a polynomial of only two variables. The previous point (2) proves that for modes satisfying $p \neq N/2, N, ...$ the splitting strength and therefore $\gamma(\pm 2p)$ are null when $\Gamma_1^0 = \Gamma_2^0$. As $\Gamma_1^0 - \Gamma_2^0$ is a common root of $\gamma(\pm 2p)$ which are one-degree polynomials, they can be recast as:*

$$\gamma(2p) = \alpha_{2p}(\Gamma_1^0 - \Gamma_2^0) \quad \textit{and} \quad \gamma(-2p) = \alpha_{-2p}(\Gamma_1^0 - \Gamma_2^0) \tag{A 7}$$

where α_{2p} and α_{-2p} depend only on the asymmetry pattern. Consequently, using equation (A 3), the splitting strength reads:

$$\mathcal{S}_0 = \sqrt{\alpha_{2p}(\Gamma_1^0 - \Gamma_2^0) \times \alpha_{N-2p}(\Gamma_1^0 - \Gamma_2^0)} = \underbrace{\sqrt{\alpha_{2p}\alpha_{N-2p}}}_{2\mathcal{K}}(\Gamma_1^0 - \Gamma_2^0) \tag{A 8}$$

Appendix B. Summary of the analytical method providing the stability map of the p^{th} azimuthal mode

This Section summarizes the analytical method to provide the stability map of the p^{th} azimuthal mode of a chamber with N burners.

• **1)** Compute the coupling factors of each burner:

$$\Gamma_i^0 = -\frac{j}{2}\frac{S_i}{S_c}\frac{\mathbb{F}^0 C_{1-\alpha}^{k^0}[jS_\alpha^{k_u^0}Z + C_\alpha^{k_u^0}] + S_{1-\alpha}^{k^0}[jC_\alpha^{k_u^0}Z - S_\alpha^{k_u^0}]}{\mathbb{F}^0 S_{1-\alpha}^{k^0}[jC_\alpha^{k_u^0} - S_\alpha^{k_u^0}Z] + C_{1-\alpha}^{k^0}[C_\alpha^{k_u^0}Z + jS_\alpha^{k_u^0}]} \tag{B 1}$$

where $\mathbb{F}^0 = \frac{c^0\rho^0}{c_u^0\rho_u^0}(1+n_i e^{j\omega^0\tau_i})$, $C_x^y = cos(xyL_i)$, $S_x^y = sin(xyL_i)$, $k^0 = \omega^0/c^0$, $k_u^0 = \omega^0/c_u^0$, Z is the upstream impedance and $\omega^0 = \frac{p\pi c^0}{L_c}$.

• **2)** Compute the total "coupling strength" $\Sigma_0 = \sum_{i=1}^N \Gamma_i^0$.

• **3)** Compute the "splitting strength" $\mathcal{S}_0$:

$$\mathcal{S}_0 = \sqrt{\sum_{i,j=1}^{N} \Gamma_i^0\Gamma_j^0 cos\left(\frac{4p\pi}{N}(j-i)\right)} = \sqrt{\gamma(-2p)\gamma(2p)} \tag{B 2}$$

where $\gamma(k)$ is the k^{th} Fourier coefficient of the asymmetry pattern.

• **4)** The p^{th} azimuthal mode is composed of two modes V^+ and V^- with the same order p but different wavenumber perturbations $\epsilon^\pm$ given by:

$$\epsilon^+ = -\frac{1}{2}\left(\Sigma_0 + \mathcal{S}_0\right) \quad \text{and} \quad \epsilon^- = -\frac{1}{2}\left(\Sigma_0 - \mathcal{S}_0\right) \tag{B 3}$$

• **5)** Then compute the complex frequency of the system from the definition of the wavenumber perturbation ($k^\pm L_c = \frac{2\pi f^\pm}{c^0} L_c = p\pi + \epsilon^\pm$) and equation (B 3):

$$f^\pm = \frac{pc^0}{2L_c} - \frac{c^0\left(\Sigma_0 \pm \mathcal{S}_0\right)}{4\pi L_c} \tag{B 4}$$

• **6)** Finally, the two components of the p^{th} azimuthal mode can have different frequencies ($f^+ \neq f^-$, non-degenerate singlets) if $\mathcal{S}_0 \neq 0$ or the same frequencies ($f^+ = f^-$, degenerate doublets) if $\mathcal{S}_0 = 0$. The growth rate of each mode is obtained from the imaginary part of the complex frequency obtained in equation (B 4):

$$\text{Growth rate}^\pm = Im(f^\pm) = -\frac{c^0}{4\pi L_c} Im\left(\Sigma_0 \pm \mathcal{S}_0\right) \tag{B 5}$$

REFERENCES

Barman, A., Barman, S., Kimura, T., Fukuma, Y. & Otani, Y. 2010 Gyration mode splitting in magnetostatically coupled magnetic vortices in an array. *J. Phys. D: Appl. Phys.* **43**, 422001.

Bauerheim, M., Cazalens, M. & Poinsot, T. 2014*a* A theoretical study of mean azimuthal flow and asymmetry effects on thermo-acoustic modes in annular combustors. *Proceedings of the 35th Combustion Institute (2014, accepted, in press)* .

Bauerheim, M., Parmentier, J.F., Salas, P., Nicoud, F. & Poinsot, T. 2014*b* An analytical model for azimuthal thermoacoustic modes in an annular chamber fed by an annular plenum. *Combustion and Flame* **161**, 1374–1389.

Berenbrink, P. & Hoffmann, S. 2001 Suppression of dynamic combustion instabilities by passive and active means, GT2001-42.

Blimbaum, J., Zanchetta, M., Akin, T., Acharya, V., J.O'Connor, Noble, D.R. & Lieuwen, T. 2012 Transverse to longitudinal acoustic coupling processes in annular combustion chambers. *International journal of spray and combustion dynamics* **4** (4), 275–298.

Borisnika, S.V. 2006 Symmetry, degeneracy and optical confinement of modes in coupled microdisk resonators and photonic crystal cavities. *IEEE J. Sel. Topics Quantum Electron* **12** (6), 1175–1182.

Bourgouin, J-F., Durox, D., Moeck, J.P., Schuller, T. & Candel, S. 2013 Self-sustained instabilities in an annular combustor coupled by azimuthal and longitudinal acoustic modes, GT2013-95010.

Busse, F.H. 1984 Oscillations of a rotating liquid drop. *J. Fluid Mech.* **142**, 1–8.

Creighton, J. A. 1982 Splitting of degenerate vibrational modes due to symmetry perturbations in tetrahedral m4 and octahedral m6 clusters. *Inorganic Chemistry* **21** (1), 1–4.

Crocco, L. 1951 Aspects of combustion instability in liquid propellant rocket motors. Part I. *J. American Rocket Society* **21**, 163–178.

Culick, F. E. C. & Kuentzmann, P. 2006 *Unsteady Motions in Combustion Chambers for Propulsion Systems*. NATO Research and Technology Organization.

Cummings, D.L. & Blackburn, D.A. 1991 Oscillations of magnetically levitated aspherical droplets. *J. Fluid Mech.* **224**, 395–416.

Davey, A. & Salwen, H. 1994 On the stability in an elliptic pipe which is nearly circular. *J. Fluid Mech.* **281**, 357–369.

Davies, P. O. A. L. 1988 Practical flow duct acoustics. *J. Sound Vib.* **124** (1), 91–115.

Dowling, A. P. 1995 The calculation of thermoacoustic oscillations. *J. Sound Vib.* **180** (4), 557–581.

Evesque, S. & Polifke, W. 2002 Low-order acoustic modelling for annular combustors: Validation and inclusion of modal coupling, GT2002-30064.

Evesque, S., Polifke, W. & Pankiewitz, C. 2003 Spinning and azimuthally standing acoustic modes in annular combustors. , AIAA paper 2003-3182.

Feng, Z.C. & Sethna, P.R. 1989 Symmetry-breaking bifurcation in resonant surface waves. *J. Fluid Mech.* **199**, 495–518.

Gelbert, G., Moeck, J.P., Paschereit, C.O. & King, R. 2012 Feedback control of unstable thermoacoustic modes in an annular rijke tube. *Control Engineering Practice* **20**, 770–782.

Guckenheimer, J. & Mahalov, A. 1992 Instability induced by symmetry reduction. *Physical Review Letter* **68**, 2257.

Guslienko, K.Y., A.N.Slavin, Tiberkevich, V. & Kim, S.K. 2008 Dynamic origin of azimuthal modes splitting in vortex-state magnetic dots. *Physical Review Letter* **24**, 247203.

Hoffmann, F., Woltersdorf, G., Perzlmaier, K., Slavin, A.N., Tiberkevich, V.S., Bischof, A., Weiss, D. & Back, C.H. 2007 Mode degeneracy due to vortex core removal in magnetic disks. *Physical Review B* **76**, 014416.

J.O'Connor & T.Lieuwen 2012*a* Influence of transverse acoustic modal structure on the forced response of a swirling nozzle flow, GT2012-70053.

J.O'Connor & T.Lieuwen 2012*b* Recirculation zone dynamics of a transversely excited swirl flow and flame. *Physics of fluids* **24** (075107).

Kammerer, M., Weigand, M., Curcic, M., Sproll, M., Vansteenkiste, A., Waeyenberge, B. Van, Stoll, H., Woltersdorf, G., Back, C.H. & Schuetz, G. 2011 Magnetic vortex core reversal by excitation of spin waves. *Nature communication* **2**, 279.

Kippenberg, T.J. 2010 Microresonators: particle sizing by mode splitting. *Nature Photonics* **4**, 9–10.

Kopitz, J., Huber, A., Sattelmayer, T. & Polifke, W. 2005 Thermoacoustic stability analysis of an annular combustion chamber with acoustic low order modeling and validation against experiment, GT2005-68797. Reno, NV, U.S.A.

Kosovichev, A.G. 1999 Inversion methods in helioseismology and solar tomography. *Journal of computational and applied mathematics* **109**, 1–39.

Krebs, W., Flohr, P., Prade, B. & Hoffmann, S. 2002 Thermoacoustic stability chart for high intense gas turbine combustion systems. *Combust. Sci. Tech.* **174**, 99–128.

Krueger, U., Hueren, J., Hoffmann, S., Krebs, W., Flohr, P. & Bohn, D. 2000 Prediction and measurement of thermoacoustic improvements in gas turbines with annular combustion systems. *J. Eng. for Gas Turbines and Power* **123** (3), 557–566.

Kumar, A. & Krousgrill, C.M. 2012 Mode-splitting and quasi-degeneracies in circular plate vibration problems: The example of free vibrations of the stator of a travelling wave ultrasonic motor. *J. Sound Vib.* **331** (26), 5788–5802.

Lavely, E.M. 1983 Theoretical investigations in helioseismology. PhD thesis, Columbia University.

Lieuwen, T. & Yang, V. 2005 *Combustion Instabilities in Gas Turbine Engines. Operational Experience, Fundamental Mechanisms and Modeling*, , vol. 210. Progress in Astronautics and Aeronautics, AIAA.

Lin, J. & Parker, R.G. 2000*a* Mesh stiffness variation instabilities in two-stage gear systems. *Journal of Vibration and Acoustics* **124**, 68–76.

Lin, J. & Parker, R.G. 2000*b* Structured vibration characteristics of planetary gears with unequally spaced planets. *J. Sound Vib.* **235** (5), 921–928.

Marble, F. E. & Candel, S. 1977 Acoustic disturbances from gas nonuniformities convected through a nozzle. *J. Sound Vib.* **55**, 225–243.

Mazzei, A., Gotzinger, S., de S. Menezes, L., Zumofen, G., Benson, O. & Sandoghdar, V. 2007 Controlled coupling of counterpropagating whispering-gallery modes by a single rayleigh scatterer: a classical problim in a quantum optical light. *Physical Review Letter* **99**, 173603.

Moeck, J.P., Paul, M. & Paschereit, C. 2010 Thermoacoustic instabilities in an annular flat rijke tube, GT2010-23577.

Nicoud, F., Benoit, L., Sensiau, C. & Poinsot, T. 2007 Acoustic modes in combustors with complex impedances and multidimensional active flames. *AIAA Journal* **45**, 426–441.

Noiray, N., Bothien, M. & Schuermans, B. 2011 Analytical and numerical analysis of

staging concepts in annular gas turbines. *Combustion Theory and Modelling* **15** (5), 585–606.

Noiray, N., Durox, D., Schuller, T. & Candel, S. 2008 A unified framework for nonlinear combustion instability analysis based on the flame describing function. *J. Fluid Mech.* **615**, 139–167.

Noiray, N. & Schuermans, B. 2013 On the dynamic nature of azimuthal thermoacoustic modes in annular gas turbine combustion chambers. *Proceedings of the Royal Society A* **469** (2151).

O'Connor, J. & T.Lieuwen 2012 Further characterization of the disturbance field in a transversely excited swirl-stabilized flame. *Journal of Engineering for Gas Turbines and Power* **134** (1), 011501.

O'Connor, J. & Lieuwen, T. 2014 (under review) Transverse combustion instabilities: acoustic, fluid mechanics and flame processes. *Progress in Energy and Combustion Sciences* .

Oefelein, J. C. & Yang, V. 1993 Comprehensive review of liquid-propellant combustion instabilities in f-1 engines. *J. Prop. Power* **9** (5), 657–677.

Palies, P. 2010 Dynamique et instabilités de combustion de flammes swirlées. Phd thesis, Ecole Centrale Paris.

Pang, L., Tetz, K.A. & Fainman, Y. 2007 Observation of the splitting of degenerate surface plasmon polariton modes in a two-dmiensional metallic nanohole array. *Applied Physics Letters* **90** (11), 111103.

Pankiewitz, C. & Sattelmayer, T. 2003 Time domain simulation of combustion instabilities in annular combustors. *ASME Journal of Engineering for Gas Turbines and Power* **125** (3), 677–685.

Parmentier, J.F., Salas, P., Wolf, P., Staffelbach, G., Nicoud, F. & Poinsot, T. 2012 A simple analytical model to study and control azimuthal instabilities in annular combustion chamber. *Combustion and Flame* **159**, 2374–2387.

Perrin, R. & Charnley, T. 1973 Group theory and the bell. *J. Sound Vib.* **31** (4), 411–418.

Pierce, A. D. 1981 *Acoustics: an introduction to its physical principles and applications*. New York: McGraw Hill.

Polifke, W., Poncet, A., Paschereit, C. O. & Doebbeling, K. 2001 Reconstruction of acoustic transfer matrices by instationnary computational fluid dynamics. *J. Sound Vib.* **245** (3), 483–510.

Poinsot, T. & Veynante, D. 2011 *Theoretical and Numerical Combustion*. Third Edition (www.cerfacs.fr/elearning).

Schuermans, B., Bellucci, V. & Paschereit, C. 2003 Thermoacoustic modeling and control of multiburner combustion systems, GT2003-38688.

Schuermans, B., Paschereit, C. & Monkewitz, P. 2006 Non-linear combustion instabilities in annular gas-turbine combustors, AIAA paper 2006-0549.

Schuller, T., Durox, D., Palies, P. & Candel, S. 2012 Acoustic decoupling of longitudinal modes in generic combustion systems. *Combustion and Flame* **159**, 1921–1931.

Selle, L., Benoit, L., Poinsot, T., Nicoud, F. & Krebs, W. 2006 Joint use of compressible large-eddy simulation and Helmholtz solvers for the analysis of rotating modes in an industrial swirled burner. *Combust. Flame* **145** (1-2), 194–205.

Sensiau, C., Nicoud, F. & Poinsot, T. 2009 A tool to study azimuthal and spinning modes in annular combustors. *Int. Journal Aeroacoustics* **8** (1), 57–68.

Silva, C.F., Nicoud, F., Schuller, T., Durox, D. & Candel, S. 2013 Combining a helmholtz solver with the flame describing function to assess combustion instability in a premixed swirled combustor. *Combustion and Flame* **160**, 1743–1754.

Silva, F., Guillemain, Ph., Kergomard, J., Mallaroni, B. & Norris, A.N. 2009 Approximation formulae for the acoustic radiation impedance of a cylindrical pipe. *Journal of Sound and Vibration* **322**, 255–263.

Simonelli, F. & Gollub, J.P. 1989 Surface wave mode interactions: effects of symmetry and degeneracy. *J. Fluid Mech.* **199**, 471–494.

Staffelbach, G., Gicquel, L.Y.M., Boudier, G. & Poinsot, T. 2009 Large eddy simulation of self-excited azimuthal modes in annular combustors. *Proc. Combust. Inst.* **32**, 2909–2916.

Stow, S. R. & Dowling, A. P. 2001 Thermoacoustic oscillations in an annular combustor, GT2001-0037, New Orleans, Louisiana.

Stow, S. R. & Dowling, A. P. 2003 Modelling of circumferential modal coupling due to helmholtz resonators, GT2003-38168, Atlanta, Georgia, USA.

Strahle, W. C. 1972 Some results in combustion generated noise. *J. Sound Vib.* **23** (1), 113–125.

Tripathy, S.C., Jain, K. & Bhatnagar, A. 2000 Helioseismic solar cycle changes and splitting coefficients. *J. Astrophys. Astr.* **21**, 349–352.

Wolf, P., Staffelbach, G., Gicquel, L.Y.M., Muller, J.D & T., Poinsot 2012 Acoustic and large eddy simulation studies of azimuthal modes in annular combustion chambers. *Combustion and Flame* **159**, 3398–3413.

Wolf, P., Staffelbach, G., Roux, A., Gicquel, L., Poinsot, T. & Moureau, V. 2009 Massively parallel LES of azimuthal thermo-acoustic instabilities in annular gas turbines. *C. R. Acad. Sci. Mécanique* **337** (6-7), 385–394.

Worth, N.A. & Dawson, J.R. 2013*a* Modal dynamics of self-excited azimuthal instabilities in an annular combustion chamber. *Combustion and Flame* **160** (11), 2476–2489.

Worth, N.A. & Dawson, J.R. 2013*b* Self-excited cricumferential instabilities in a model annular gas turbine combustor: global flame dynamics. *Proceedings of the Combustion Institute* **34**, 3127–3134.